METHODS AND APPROACHES

Action potentials in *Xenopus* oocytes triggered by blue light

Florian Walther[1]*, Dominic Feind[1]*, Christian vom Dahl[1]*, Christoph Emanuel Müller[1], Taulant Kukaj[1], Christian Sattler[1], Georg Nagel[2], Shiqiang Gao[2], and Thomas Zimmer[1]

Voltage-gated sodium (Na⁺) channels are responsible for the fast upstroke of the action potential of excitable cells. The different α subunits of Na⁺ channels respond to brief membrane depolarizations above a threshold level by undergoing conformational changes that result in the opening of the pore and a subsequent inward flux of Na⁺. Physiologically, these initial membrane depolarizations are caused by other ion channels that are activated by a variety of stimuli such as mechanical stretch, temperature changes, and various ligands. In the present study, we developed an optogenetic approach to activate Na⁺ channels and elicit action potentials in *Xenopus laevis* oocytes. All recordings were performed by the two-microelectrode technique. We first coupled channelrhodopsin-2 (ChR2), a light-sensitive ion channel of the green alga *Chlamydomonas reinhardtii*, to the auxiliary β1 subunit of voltage-gated Na⁺ channels. The resulting fusion construct, β1-ChR2, retained the ability to modulate Na⁺ channel kinetics and generate photosensitive inward currents. Stimulation of *Xenopus* oocytes coexpressing the skeletal muscle Na⁺ channel $Na_v1.4$ and β1-ChR2 with 25-ms lasting blue-light pulses resulted in rapid alterations of the membrane potential strongly resembling typical action potentials of excitable cells. Blocking $Na_v1.4$ with tetrodotoxin prevented the fast upstroke and the reversal of the membrane potential. Coexpression of the voltage-gated K⁺ channel $K_v2.1$ facilitated action potential repolarization considerably. Light-induced action potentials were also obtained by coexpressing β1-ChR2 with either the neuronal Na⁺ channel $Na_v1.2$ or the cardiac-specific isoform $Na_v1.5$. Potential applications of this novel optogenetic tool are discussed.

Introduction

Voltage-gated sodium (Na⁺) channels initiate the rapid upstroke of action potentials (APs) in excitable cells. These channels are heteromultimeric proteins consisting of a large pore-forming α subunit (∼260 kD) and smaller accessory β subunits (Goldin et al., 2000; Goldin, 2001; Brackenbury and Isom, 2011; Catterall, 2017). The α subunit determines the main electrophysiological and pharmacological properties of a given Na⁺ channel complex, while β subunits modulate the function of α subunits.
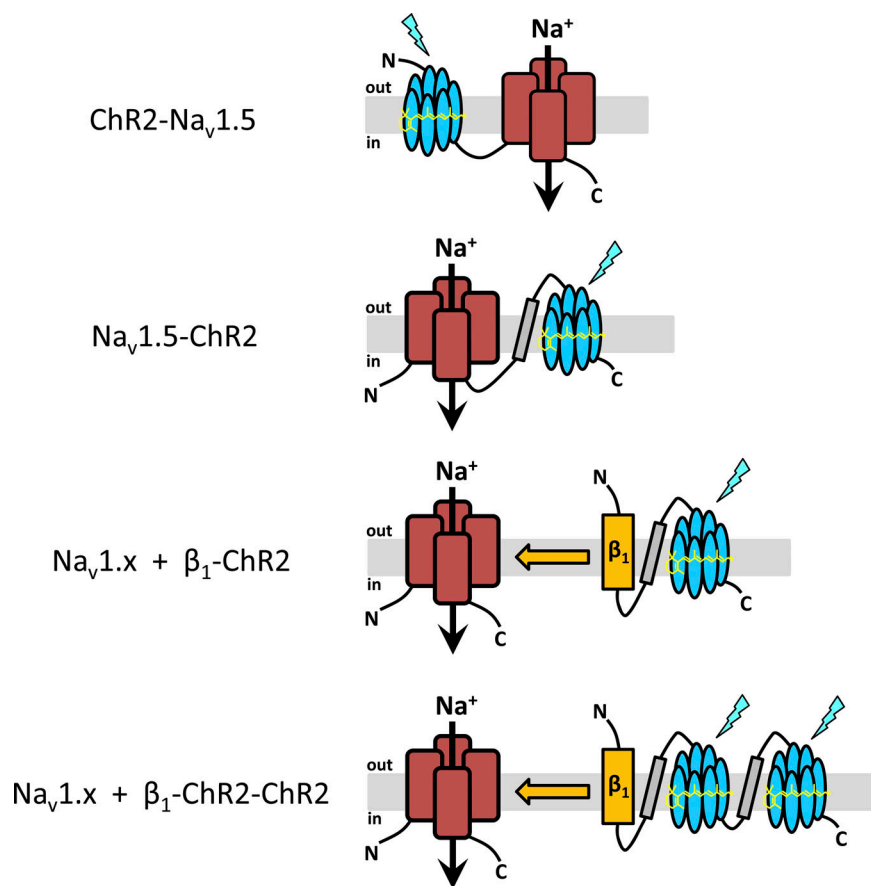
The α subunit is composed of four homologous domains (DI–DIV) that are connected by intracellular linkers. Each domain contains six transmembrane segments. The fourth segment (S4) of each domain is an essential element of the voltage sensor. A depolarizing voltage pulse leads to a transient outward movement of the S4s, thereby initiating the opening of the pore. The large Na⁺ conductance of 10–30 pS (Sigworth and Neher, 1980; Bezanilla, 1987) finally allows for the fast AP upstroke. The ensuing transition from the open to the inactivated state occurs

within a few milliseconds after opening. This so-called open-state inactivation is mediated by an intracellularly located inactivation gate, formed by the DIII–DIV linker. The termination of the Na⁺ influx and the activation of voltage-gated K⁺ channels limit the AP amplitude and allow for fast repolarization. Nine different functional Na⁺ channel α subunits have been identified by electrophysiological recordings, biochemical purification, and cloning studies (Goldin et al., 2000; Goldin, 2001). The α subunits $Na_v1.1$, $Na_v1.2$, and $Na_v1.3$ are the major isoforms of the central nervous system, $Na_v1.4$ is mainly expressed in skeletal muscle, $Na_v1.5$ is the cardiac isoform, $Na_v1.6$ is widely expressed in various neurons of the central and peripheral nervous system, and $Na_v1.7$, $Na_v1.8$, and $Na_v1.9$ are expressed primarily in the peripheral nervous system. According to their binding affinity for the puffer fish poison tetrodotoxin (TTX), voltage-gated Na⁺ channels have been classified into two pharmacologically different groups: cardiac $Na_v1.5$ as well as neuronal $Na_v1.8$ and $Na_v1.9$ channels are resistant to nanomolar TTX concentrations

Figure 1. **Experimental strategy.** The purpose of our study was to elicit light-induced APs not by coexpression of wild type ChR2 with voltage-gated Na⁺ channels, but by coupling ChR2 either directly to Na$_v$1.5 (ChR2-Na$_v$1.5, Na$_v$1.5-ChR2) or to the accessory β1 subunit (β1-ChR2, β1-ChR2-ChR2). The seven transmembrane regions of ChR2 (blue), the four large domains of voltage-gated Na⁺ channels (red), the β1 subunit (orange), and the membrane-spanning region of the human H⁺/K⁺ATPase (gray) are illustrated. In Na$_v$1.5-ChR2, β1-ChR2, and β1-ChR2-ChR2, peptide [GGGS]$_3$ was incorporated into all linker regions (symbolized by a black line). For detailed amino acid composition of the constructs, see Materials and methods.
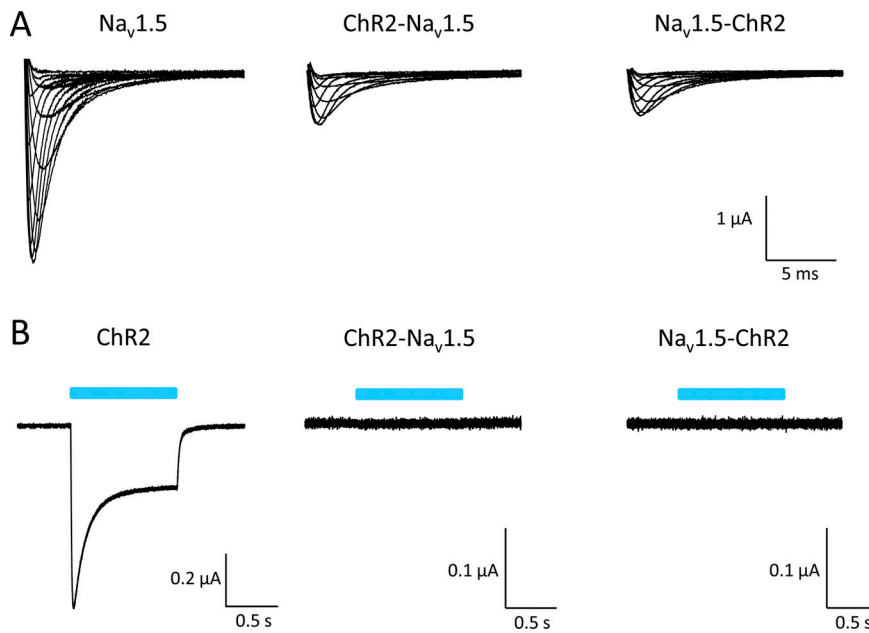
(half-maximal inhibitory concentration [IC$_{50}$], ~1–6 µM; Gellens et al., 1992; Goldin, 2001). The other neuronal Na⁺ channels as well as the skeletal muscle channel Na$_v$1.4 are highly sensitive toward TTX (IC$_{50}$ ~10 nM; Goldin, 2001).

Four distinct β subunits have been found in various excitable tissues. They are glycosylated membrane proteins composed of a larger N-terminal extracellular region that is connected via a single transmembrane segment to a smaller C-terminal intracellular domain. The β1 subunit is expressed in all excitable tissues including brain, dorsal root ganglia, sciatic nerve, spinal cord, skeletal muscle, and throughout the heart (Sutkowski and Catterall, 1990; Isom et al., 1992; Brackenbury and Isom, 2011). It functionally interacts with multiple Na⁺ channel α subunits (Patton et al., 1994) shifts steady-state gating, accelerates Na⁺ current decay kinetics, and facilitates recovery from inactivation of Na⁺ channel α subunits (Isom et al., 1992; Nuss et al., 1995; Zimmer and Benndorf, 2002).

Channelrhodopsins represent the only directly light-gated ion channels in nature (Nagel et al., 2002, 2003; Schneider et al., 2015). The cDNAs for channelrhodopsin-1 and channelrhodopsin-2 (ChR2) were discovered in a data bank of expressed sequence tags from the green alga *Chlamydomonas reinhardtii* and identified as partially homologous to the light-driven H⁺-pump bacteriorhodopsin. Both proteins were characterized in detail after heterologous expression in oocytes of *Xenopus laevis* (Nagel et al., 2002, 2003). ChR2 was also successfully expressed in mammalian cells and shown to confer light-induced depolarization via light-activatable cation permeability in these cells

(Nagel et al., 2003). This seven-transmembrane helix protein is mainly permeable for protons, less for sodium and potassium, and also for calcium (Nagel et al., 2003). It consists of an opsin as the apoprotein and the chromophore retinal, which is connected via protonated Schiff-base linkage to lysine 257. Naturally, ChR2 occurs in dimers; the respective interaction is mediated by helices 3 and 4 and a disulfide bond of cysteines on the extracellular N-termini (Volkov et al., 2017). The pore is formed by helices 1, 2, 3, and 7. Blue-light illumination causes retinal isomerization leading to conformational changes that open the pore for cation influx (Berndt et al., 2011). The photocycle for ChR2 can be explained by a four-state model considering two conducting and two dark nonconducting states (Schneider et al., 2015; Deisseroth and Hegemann, 2017).

Since five groups independently expressed ChR2 in neurons and showed strong light-effects, the new field of optogenetics rapidly evolved, because of the opportunity to control specific cells noninvasively by blue light (Boyden et al., 2005; Li et al., 2005; Nagel et al., 2005; Bi et al., 2006; Ishizuka et al., 2006). In this novel research field, endogenous voltage-gated ion channels of excitable cells are activated by ChR2-mediated membrane depolarization, resulting in blue light–triggered APs. Driven by the potential of this method, scientists mutated ChR2 to obtain variants with increased potency and light sensitivity (Berndt et al., 2011; Ullrich et al., 2013; Schneider et al., 2015). One of the mutants, T159C, produces large photocurrents by stabilizing the Schiff-base linkage of retinal to lysine 257 (Ullrich et al., 2013). Despite all the important progress in recent years, ChR2

Walther et al.
Light-induced action potentials in *Xenopus* oocytes

Journal of General Physiology   2 of 16
https://doi.org/10.1085/jgp.201912489

Figure 2. Electrophysiological test for functional expression of ChR-Na$_v$1.5 and Na$_v$1.5-ChR2 in *Xenopus* oocytes. (A) Representative whole-cell currents generated by wild type Na$_v$1.5, ChR2-Na$_v$1.5, and Na$_v$1.5-ChR2 at test potentials between −45 and +20 mV. Injected amount of cRNA per oocyte: 0.1 ng Na$_v$1.5, 10 ng ChR2-Na$_v$1.5, and 10 ng Na$_v$1.5-ChR2. Peak current density for Na$_v$1.5 was 1.56 ± 0.1 µA (n = 10). Current reduction was similar in ChR2-Na$_v$1.5 and Na$_v$1.5-ChR2 (0.59 ± 0.08 µA with n = 21 versus 0.71 ± 0.07 µA with n = 27, respectively; $P < 0.05$ versus Na$_v$1.5). **(B)** None of the ChR2 fusions responded to a 1-s blue-light pulse. Injected amount of cRNA per oocyte: 0.2 ng ChR2, 10 ng ChR2-Na$_v$1.5, and 10 ng Na$_v$1.5-ChR2.

and all its variants are still characterized by an extremely small conductance that is too small to be determined experimentally. Estimates assume a single-channel conductance of 40–60 fS (Nagel et al., 2003; Feldbauer et al., 2009), which is almost three orders of magnitude smaller than the conductance of a voltage-gated Na$^+$ channel. Additionally, ChR2 does not have any localization preference in the plasma membrane of target cells, i.e., it does not specifically localize at regions with a high density of voltage-gated Na$^+$ channels, like the axon hillock of neurons or the intercalated disc region of cardiac myocytes.

In the present study, we introduce an optogenetic tool by combining ChR2-mediated membrane depolarization with the vast conductance of a voltage-gated Na$^+$ channel. By direct coupling of ChR2 to one of the Na$^+$ channel β subunits, we were able to evoke artificial APs in *Xenopus* oocytes coexpressing brain-, muscle-, or heart-type Na$^+$ channel α subunits. This enables us to shape APs in naturally unexcitable cells, as similarly shown recently by a current injection method (Corbin-Leftwich et al., 2016, 2018). Our novel optogenetic approach with β1-ChR2 provides the potential for noninvasive excitation.

Materials and methods
Plasmids and recombinant DNA procedures
For the expression of Na$_v$1.2 (brain IIA; GenBank accession nos. X03639 and X61149), Na$_v$1.4 (GenBank accession no. AJ278787), Na$_v$1.5 (GenBank accession no. M77235), β1 (GenBank accession no. M91808), K$_v$2.1 (GenBank accession no. X68302), and ChR2 (GenBank accession no. AF461397), the following plasmids were used: pNa200 (Auld et al., 1988; kindly provided by Dr. A.L. Goldin, University of California, Irvine, CA), pSP64T-mNa$_v$1.4 (Zimmer and Benndorf, 2007), pTSV40G-hNa$_v$1.5 (Walzik et al., 2011), pGEM-β1 (Zimmer and Benndorf, 2002), pGEMHE-hK$_v$2.1 (h-DRK1; Koopmann et al., 2001), and pGEMHE-ChR2-T159C:: YFP (Berndt et al., 2011; Ullrich et al., 2013). The ChR2-T159C mutant showing an enhanced binding affinity to the endogenous retinal of oocytes was used throughout the study.

The ChR2-Na$_v$1.5 fusion was constructed by overlapping PCR. First, we amplified the ChR2-T159C cDNA, encoding M1 to V309, and a short N-terminal hNa$_v$1.5 fragment, encoding M1 to K98, in separate reactions. The second recombinant PCR step resulted in a 1.3-kb fragment that was digested by HindIII (incorporated into the ChR2 forward primer) and SdaI (present in the hNa$_v$1.5
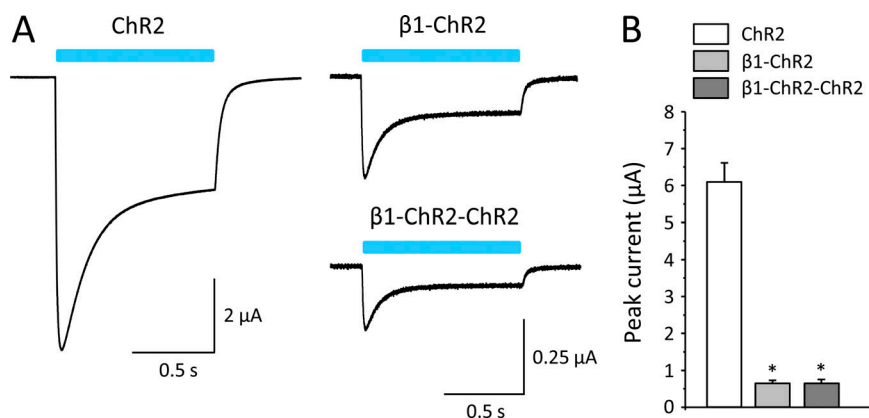
Figure 3. Whole-cell currents through ChR2, β1-ChR2, and β1-ChR2-ChR2 channels. (A) Linkage of the C-terminus of the β1 subunit to the N-terminus of the ChR2 resulted in typical light-induced inward currents in the voltage-clamp mode. The plateau current relative to the transient current was similar for all three channels (52.9 ± 7.6% in ChR2, 42.8 ± 8.2% in β1-ChR2, and 42.0 ± 10.8% in β1-ChR2-ChR2). **(B)** Currents were significantly reduced when injecting 10 ng cRNA per oocyte. Notably, coupling of a second ChR2 did not alter expression (possible reasons are discussed in the text). Number of measurements were n = 27 (ChR2), n = 20 (β1-ChR2), and n = 21 (β1-ChR2-ChR2; *, $P < 0.05$ versus ChR2). Error bars represent SEM.
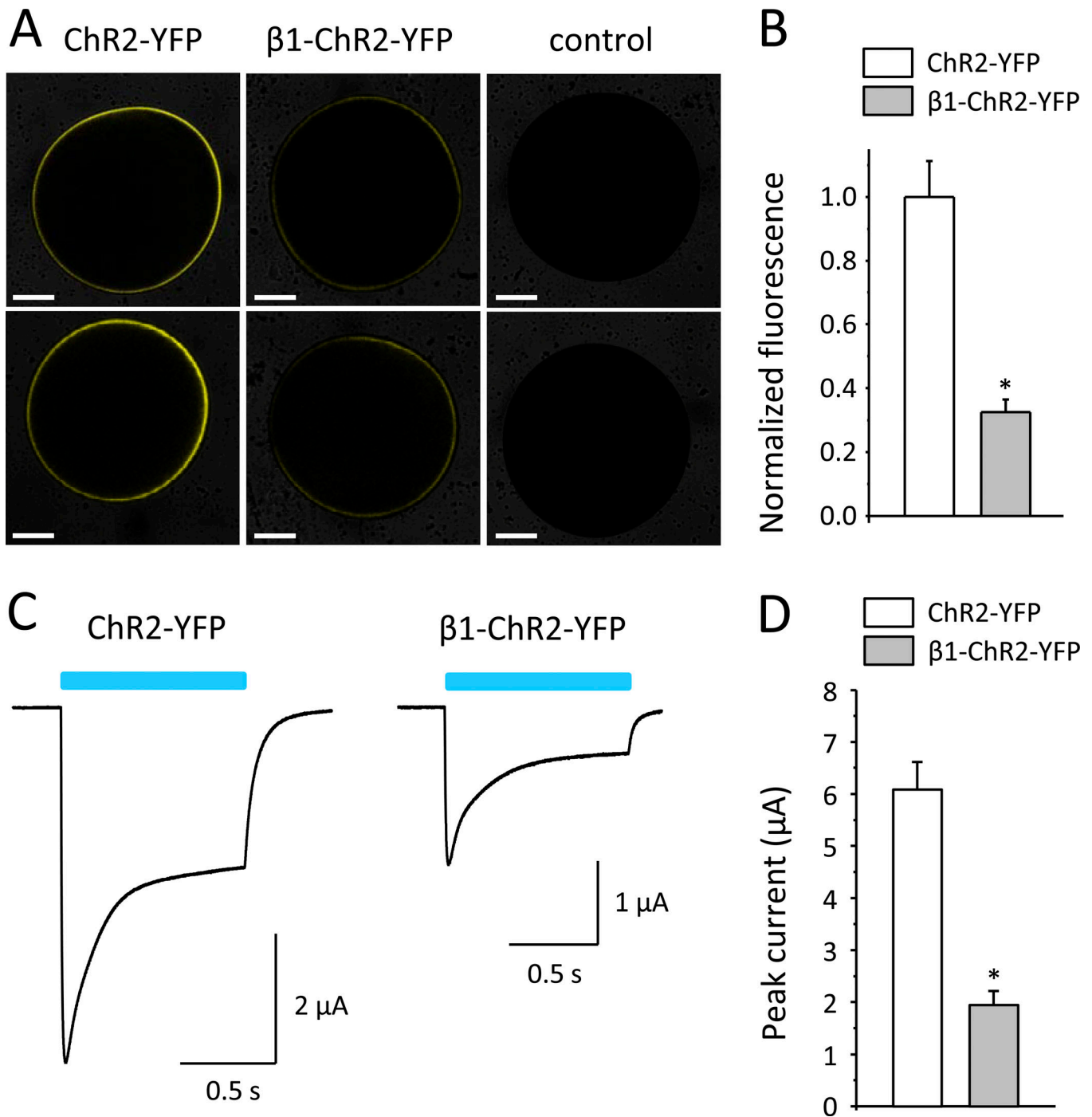
Figure 4. Comparison of membrane fluorescence and photocurrents in *Xenopus* oocytes expressing ChR2-YFP and β1-ChR2-YFP. (A) Representative fluorescence images of *Xenopus* oocytes. Noninjected control oocytes showed only faint background fluorescence. Scale bars: 0.25 mm. **(B)** Normalized fluorescence intensities. Data points are from three different oocyte batches with *n* = 22 for ChR2-YFP and *n* = 19 for β1-ChR2-YFP (*, P < 0.05 versus ChR2-YFP). **(C)** Representative whole-cell currents through ChR2-YFP and β1-ChR2-YFP. **(D)** Peak current amplitudes. Number of measurements were *n* = 27 for ChR2-YFP and *n* = 26 for β1-ChR2-YFP (*, P < 0.05 versus ChR2-YFP). Four different oocyte batches were used. Error bars represent SEM.

cDNA). Both sites were used to insert the chimeric fragment into pTSV40G-hNa$_v$1.5. The resulting plasmid, pTSV40G-ChR-hNa$_v$1.5, was expected to encode the following channel protein: ChR2/T159C$_{M1-V309}$-hNa$_v$1.5$_{M1-V2016}$ (ChR-Na$_v$1.5 in Fig. 1).

For the construction of β1-ChR2, first we purchased a synthetic DNA fragment (Invitrogen) coding for the following

chimeric protein: full-length human Na$^+$ channel β1 subunit (hβ1; GenBank accession no. L16242), linker GGGS-GGGS-GGGS ([GGGS]$_3$), transmembrane region A$_2$ to N$_{103}$ of the β subunit of the human H$^+$/K$^+$-ATPase (hβHK$_{A2-N103}$; GenBank accession no. NM_000705), and linker region [GGGS]$_3$. The coding region of ChR2 mutant T159C (ChR2/T159C), lacking the putative signal
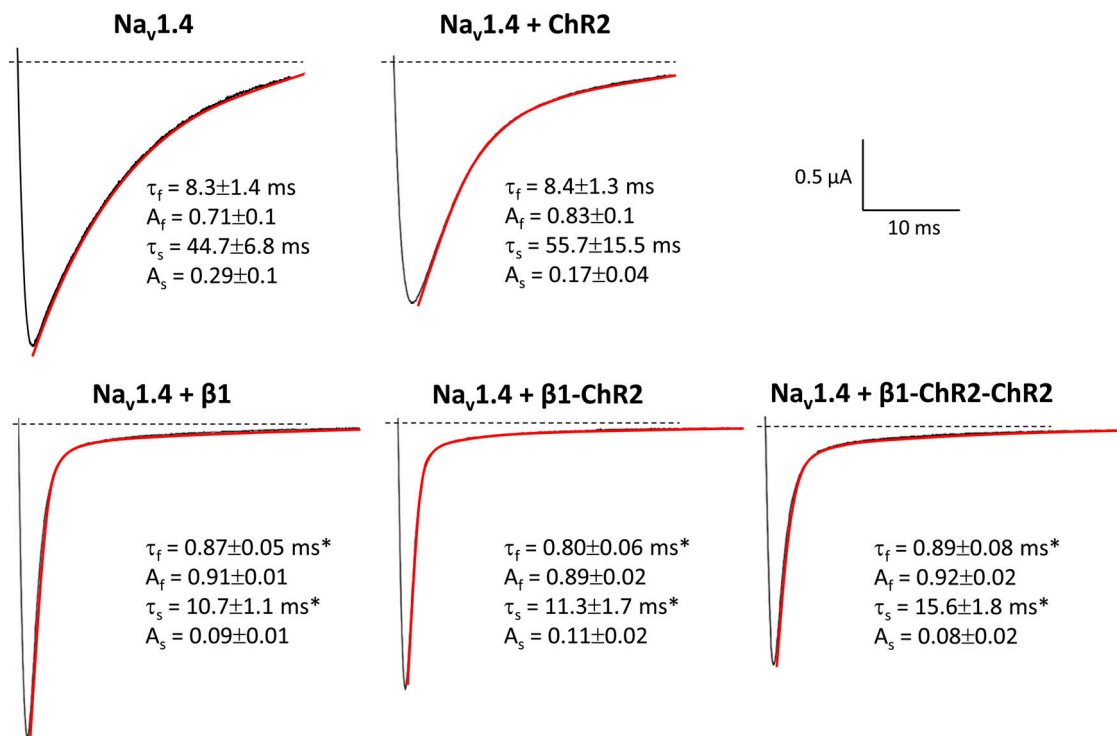
Figure 5. **Representative Na$_v$1.4 current traces at a test potential of −10 mV in *Xenopus* oocytes.** Coexpression of β1 resulted in a faster decay of macroscopic Na$^+$ currents through Na$_v$1.4 channels. To better illustrate the effect on inactivation, we selected whole-cell currents with similar amplitude. Current traces were fitted (red) using a biexponential function: $I = A_f \times \exp(-t/\tau_f) + A_s \times \exp(-t/\tau_s)$, where τ_f and τ_s are the fast and slow time constants, and A_f and A_s are the corresponding amplitudes. Both fast and slow time constants, τ_f and τ_s, were significantly shorter. This well-known β1 property remained preserved in β1-ChR2 and β1-ChR2-ChR2 and was not obtained when coexpressing ChR2 (top). Values for τ_f, A_f, τ_s, and A_s are from at least six different measurements (*, significantly different versus Na$_v$1.4, $P < 0.05$). This typical acceleration of inactivation was also obtained at all other test pulses.

sequence M$_1$ to V$_{23}$ and the C-terminal region N$_{310}$ to E$_{737}$, was finally coupled in-frame by a recombinant PCR approach. The resulting construct was subcloned into the BamHI/XbaI sites of oocyte expression vector pGEMHEnew, resulting in pGEM-β1-ChR2. The expected amino acid sequence of β1-ChR2 is as follows: hβ1$_{M1-E218}$-[GGGS]$_3$-hβHK$_{A2-N103}$-[GGGS]$_3$-ChR2/T159C$_{N24-V309}$ (β1-ChR2 in Fig. 1). The sequence of the YFP was coupled in-frame to the C-terminus of β1-ChR2 by recombinant PCR, thereby incorporating also a Golgi-to-plasma membrane trafficking signal (Hofherr et al., 2005) and an ER export motif (Stockklausner et al., 2001). The resulting plasmid pGem-β1-ChR2-YFP was analyzed by suitable restriction enzymes and DNA sequencing. The expected amino acid sequence of the coding region is as follows: hβ1$_{M1-E218}$-[GGGS]$_3$-hβHK$_{A2-N103}$-[GGGS]$_3$-ChR2/T159C$_{N24-V309}$-[KSRITSEGEYIPLDQIDINVVDTSSR]-YFP$_{M1-K239}$-[SRFCYENEV].

To obtain β1-ChR2-ChR2, we first exchanged the stop codon in pGEM-β1-ChR2 by a short sequence coding for linker region GGGSR using a respectively designed PCR primer. The resulting vector, pGEM-β1-ChR2*, still contained the XbaI and HindIII sites to allow for downstream coupling of the second ChR2 cDNA. The respective 1.3-kb fragment, separately amplified by PCR from pGEM-β1-ChR2, was expected to encode for the following amino acid sequence: [GGGS]$_2$-hβHK$_{A2-N103}$-[GGGS]$_3$-ChR2/T159C$_{N24-V309}$. An XbaI site was incorporated in the forward and a HindIII site in the reverse primer so that the PCR

fragment obtained could be finally subcloned into pGEM-β1-ChR2*. The resulting plasmid, pGEM-β1-ChR2-ChR2, was used to produce the β1-ChR2-ChR2 cRNA and finally the following channel protein: hβ1$_{M1-E218}$-[GGGS]$_3$-hβHK$_{A2-N103}$-[GGGS]$_3$-ChR2/T159C$_{N24-V309}$-GGGSR-[GGGS]$_2$-hβHK$_{A2-N103}$-[GGGS]$_3$-ChR2/T159C$_{N24-V309}$ (β1-ChR2-ChR2 in Fig. 1).

The Na$_v$1.5-ChR2 fusion was also constructed by overlapping PCR. First, we amplified in separate reactions a 0.4-kb fragment (expected to encode hNa$_v$1.5$_{R2012-V2016}$-[GGGS]$_3$-hβHK$_{A2-N103}$-[GGGS]$_3$-ChR2/T159C$_{N24-E31}$) using pGEM-β1-ChR2, a 0.9-kb fragment (expected to encode ChR2/T159C$_{N24-V309}$) using pGEM-β1-ChR2, and a short C-terminal hNa$_v$1.5 fragment (expected to encode hNa$_v$1.5$_{R1897-V2016}$-GGGSG) using expression plasmid pTSV40G-hNa$_v$1.5. The recombinant PCR step resulted in a 1.6-kb fragment that was digested by Tth111I (present in the hNa$_v$1.5 cDNA) and NotI (incorporated into the ChR2 reverse primer downstream to the stop codon). Both restriction sites were used to insert the chimeric fragment into pTSV40G-hNa$_v$1.5. The resulting plasmid, pTSV40G-hNa$_v$1.5-ChR2, was used to produce the Na$_v$1.5-ChR2 cRNA and finally the following channel protein: hNa$_v$1.5$_{M1-V2016}$-[GGGS]$_3$-hβHK$_{A2-N103}$-[GGGS]$_3$-ChR2/T159C$_{N24-V309}$ (Na$_v$1.5-ChR2 in Fig. 1).

A thermostable DNA polymerase with proofreading activity was used for all PCR reactions (Pfu DNA polymerase, Promega). The correctness of PCR-derived sequences was confirmed by DNA sequencing (Seqlab Microsynth).

Table 1. **Modulation of Na$_v$1.4 channels in *Xenopus* oocytes by β1, β1-ChR2, and β1-ChR2-ChR2**

Channel	Steady-state activation		Steady-state inactivation		Recovery from inactivation			
	V_m (mV)	s (mV)	V_h (mV)	s (mV)	$τ_f$ (ms)	A_f	$τ_s$ (ms)	A_s
Na$_v$1.4	−19.8 ± 0.7	1.9 ± 0.3	−36.3 ± 2.0	5.3 ± 0.2	1.11 ± 0.57	0.46 ± 0.10	153 ± 10.3	0.54 ± 0.10
Na$_v$1.4 + ChR2	−19.7 ± 0.9	2.0 ± 0.2	−40.0 ± 2.2	5.4 ± 0.2	1.19 ± 0.65	0.63 ± 0.10	218 ± 3.51	0.37 ± 0.10
Na$_v$1.4 + β1	−24.1 ± 0.8[a]	2.9 ± 0.3	−48.4 ± 4.0[a]	4.7 ± 0.6	0.39 ± 0.02	0.99 ± 0.003[a]	17.6 ± 4.27[a]	0.01 ± 0.003[a]
Na$_v$1.4 + β1-ChR2	−24.2 ± 1.7[a]	2.3 ± 0.4	−46.0 ± 1.7[a]	3.8 ± 0.1[a]	0.37 ± 0.01	0.99 ± 0.002[a]	21.8 ± 2.36[a]	0.01 ± 0.002[a]
Na$_v$1.4 + β1-ChR2-ChR2	−22.8 ± 0.7[a]	2.6 ± 0.3	−46.1 ± 1.0[a]	3.8 ± 0.1[a]	0.42 ± 0.04	0.99 ± 0.002[a]	19.7 ± 5.96[a]	0.01 ± 0.002[a]

Coexpression of β1 as well as both ChR2-coupled β1 subunits significantly shifted the steady-state activation and inactivation curves toward hyperpolarized potentials. Moreover, the amplitudes of the fast recovery time constant (A_f) were increased, and the shorter time constants ($τ_s$) as well as the respective amplitudes (A_s) were clearly reduced, further indicating that coupling of ChR2 did not alter typical features of the β1 subunit. For equations and abbreviations, see Materials and methods.
[a]P < 0.05 versus Na$_v$1.4 (with *n* = 4–8).

Heterologous expression in *Xenopus* oocytes

In vitro transcription was done using the mMESSAGE mMA-CHINE T7 Transcription Kit (Life Technologies) after linearization with NotI, XbaI, or NheI (pGEM-derived plasmids, pNa200, and pTSV40G-hNa$_v$1.5), and the mMESSAGE mMACHINE SP6 Transcription Kit (Life Technologies) after linearization with NotI (pSP64T-mNa$_v$1.4). We used pGEMHE-ChR2-T159C::YFP as the ChR2 control plasmid (NheI digestion and T7 promoter for in vitro transcription). The quality of the cRNA was checked by agarose gel electrophoresis; the concentration was determined using a NanoDrop 2000c spectrophotometer (Thermo Scientific). *Xenopus* oocytes obtained from EcoCyte Bioscience were injected with 50–70 nl of cRNA and incubated at 18°C for 48–72 h in Barth medium (in mM: 84 NaCl, 1 KCl, 2.4 NaHCO$_3$, 0.82 MgSO$_4$, 0.33 Ca(NO$_3$)$_2$, 0.41 CaCl$_2$, and 7.5 Tris/HCl, pH 7.4) containing 1 µM all-trans Retinal (Sigma). At least four different batches of oocytes were tested for each construct and construct combination.

Electrophysiological recordings and fluorescence imaging

All recordings were performed at room temperature with the two-microelectrode technique using the TEC-05-S amplifier from npi Electronic Instruments, as previously described (Gütter et al., 2013). The following bath solution was used (in mM): 96 NaCl, 2 KCl, 1.8 CaCl$_2$, 1 MgCl$_2$, and 10 HEPES/KOH, pH 7.4 (Gütter et al., 2013). Glass microelectrodes were filled with 3 M KCl. Microelectrode resistance was between 0.1 and 0.6 MΩ. Membrane resistance of injected oocytes was calculated from the leak current difference at −120 and −80 mV in the voltage-clamp mode. Oocytes with a resistance <100 kΩ were excluded (for mean values and oocyte variability, see Table S1 and Table S2). Recording and analysis of the data were performed on a
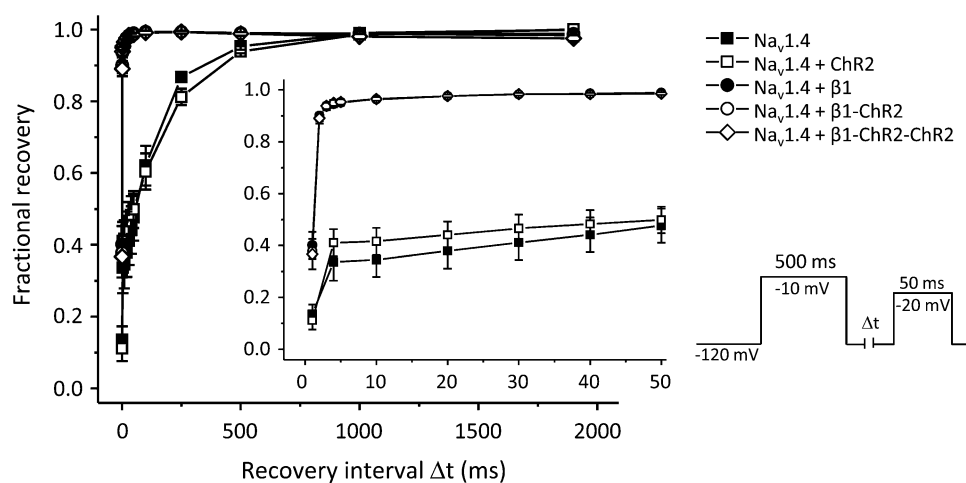
Figure 6. **Acceleration of recovery from inactivation of Na$_v$1.4 by β1, β1-ChR2, and β1-ChR2-ChR2.** The respective voltage protocol is shown on the right. During the first pulse (500 ms at −10 mV), Na$_v$1.4 channels were activated; subsequently they accumulated in the inactivated state. During the time interval Δt, channels were allowed to recover at −120 mV. The second test pulse to −20 mV was used to determine the respective fraction of non-inactivated channels. Coexpression of β1 as well as both ChR2-coupled β1 subunits accelerated this recovery process. Data points are from two oocyte batches and four to eight different recordings. For statistics, see Table 1. Error bars represent SEM.
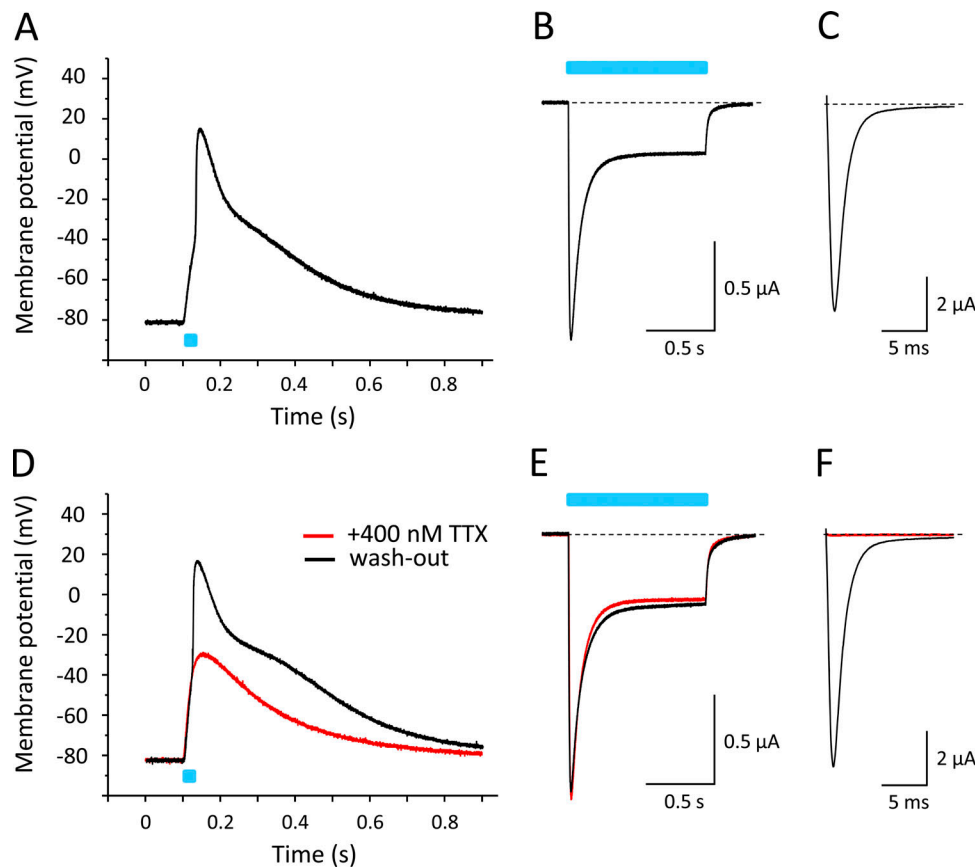
Figure 7. **Light-induced APs in *Xenopus* oocytes coexpressing Na$_v$1.4 and β1-ChR2.** All recordings shown were performed on a single oocyte. Light pulses are illustrated as blue bars. **(A)** Current-clamp recording. The membrane potential was set to –80 mV, and the change of membrane voltage was followed on a 25-ms light pulse delivered to the whole oocyte. For AP variability and for detailed statistics, see Fig. S1 and Table S1. **(B)** Corresponding whole-cell current through β1-ChR2 channels recorded in the voltage-clamp mode. Pulse duration was 1 s. **(C)** Na$_v$1.4 whole-cell current of the same oocyte recorded in the voltage-clamp mode (holding potential, –120 mV; test pulse, –25 mV). **(D)** Current-clamp recording in the presence of 400 nM TTX (red). The remaining depolarization was due to ChR2 activity. Washout restored the fast upstroke to nearly +20 mV (black). **(E)** TTX did not affect β1-ChR2 activity (voltage-clamp recording as in B). **(F)** Na$_v$1.4 channels were completely blocked in the presence of 400 nM TTX (voltage-clamp mode as in C). Black line shows the Na$^+$ current after washout of TTX.

personal computer with ISO3 software (MFK). The sampling rate was 5 kHz, except for the whole-cell Na$^+$ channel measurements (20–50 kHz). Student's *t* test was used to test for statistical significance. Statistical significance was assumed for P < 0.05.

Currents through Na$^+$ channels were elicited by test potentials from –80 to 50 mV in 5- or 10-mV increments at a pulsing frequency of 1.0 Hz (holding potential –120 mV). Steady-state activation (m_∞) was evaluated by fitting the Boltzmann equation $m_\infty = \{1 + \exp[-(V - V_m)/s]\}^{-1}$ to the normalized conductance as function of voltage. Steady-state inactivation (h_∞) was determined with a double-pulse protocol consisting of 500-ms prepulses to voltages between –140 and –30 mV followed by a constant test pulse of 10-ms duration to –20 mV at a pulsing frequency of 0.5 Hz. The amplitude of peak I_{Na} during the test pulse was normalized to the maximum peak current and plotted as function of the prepulse potential. Data were fitted to the Boltzmann equation $h_\infty = \{1 + \exp[(V - V_h)/s]\}^{-1}$, where V is the test potential, V_m and V_h are the midactivation and mid-inactivation potentials, respectively, and s is the slope factor in

mV. Recovery from inactivation was determined with a double-pulse protocol consisting of a 500-ms prepulse to –10 mV, a variable recovery interval at –120 mV, and a second test pulse of 20 ms duration to –20 mV at a pulsing frequency of 0.2 Hz. Recovery of Na$_v$1.4 channels was analyzed by fitting data using the two-exponential equation $I = 1 - [A_1 \times \exp(-t/\tau_1) + A_2 \times \exp(-t/\tau_2)]$, where I is the normalized current, t is the recovery time, and τ_1 and τ_2 are time constants of fast- and slow-recovering components, respectively. Currents through K$^+$ channels were elicited by test potentials from –70 to 50 mV in 10-mV increments at a pulsing frequency of 1.0 Hz (holding potential –80 mV).

Blue-light pulses for the activation of ChR2 (maximum at 472 nm) were delivered to the oocytes via a light guide mounted to a self-made LED device (internal workshop). In voltage-clamp experiments, the holding potential was set to –80 mV. APs were recorded in the current-clamp mode after setting the resting membrane potential from approximately –30 to –80 mV by an appropriate current injection. Light intensity was measured by the LaserCheck power meter from Coherent. Measurements resulted in 7.1 mW/mm². Light pulses were
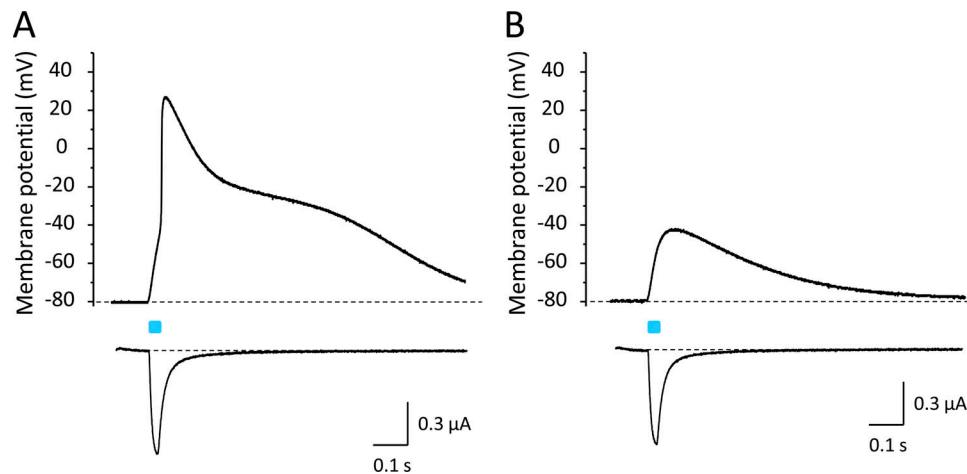
Figure 8. **Light-induced changes of membrane potential and membrane current upon coexpression of Na$_v$1.4 and β1-ChR2 in *Xenopus* oocytes. (A)** Current-clamp and voltage-clamp recording in the absence of TTX. The membrane potential was set to –80 mV, and both the change of membrane voltage and the inward current were followed on a 25-ms light pulse delivered to the whole oocyte. **(B)** Current-clamp and voltage-clamp recording in the presence of 400 nM TTX (same oocyte as in A). The toxin did not reduce the light-triggered inward current recorded at –80 mV. Pulsing from –120 to –35 mV in the voltage-clamp mode revealed that the toxin blocked >99% of Na$_v$1.4 channels, similarly as shown in Fig. 7.

elicited by the respective trigger function implemented in ISO3.

To analyze cell surface expression of YFP-labeled ChR2 and β1-ChR2, oocyte images were recorded under identical settings by a confocal laser-scanning microscope (LSM710; Carl Zeiss) using an EC Plan-Neofluar 10×/0.3 M27 objective. YFP in both fusion proteins was excited by the 514-nm line of the argon laser and detected in the 517–581-nm range. Received 12-bit images show a confocal slice of an oocyte. The mean intensity of the whole images was analyzed by the implemented tool in the ZEN 2010 software. Mean intensity of noninjected cells was subtracted.

Online supplemental material

Figs. S1 and S2 show superimposed current-clamp recordings for Na$_v$1.4- and Na$_v$1.5-mediated APs in *Xenopus* oocytes, respectively. Both figures illustrate the variability of the light-induced APs. Table S1 and Table S2 show the corresponding values for the oocyte membrane resistance, the size of the photocurrent, the peak Na$^+$ current, the K$^+$ current, and several AP parameters (threshold, overshoot, 10–90% rise time, and AP duration for two above-threshold voltages).

Results

Direct coupling of ChR2 to Na$_v$1.5

To place ChR2 next to a sodium channel, we coupled ChR2 first to the N- or C-terminus of the human cardiac voltage-gated Na$^+$ channel Na$_v$1.5, resulting in ChR2-Na$_v$1.5 and Na$_v$1.5-ChR2, respectively (Fig. 1). In ChR2-Na$_v$1.5, the C-terminus of ChR2 was directly linked to the N-terminus of Na$_v$1.5. In Na$_v$1.5-ChR2, we incorporated the transmembrane N-terminal helix of the β subunit of the human H$^+$/K$^+$-ATPase as a membrane-spanning region between the intracellularly exposed C-terminus of Na$_v$1.5 and the extracellular N-terminus of ChR2, as successfully demonstrated in an earlier study (Kleinlogel et al., 2011).

Expression in *Xenopus* oocytes of both ChR2-Na$_v$1.5 and Na$_v$1.5-ChR2 resulted in voltage-activated Na$^+$ currents (Fig. 2 A). However, peak Na$^+$ current amplitudes were significantly reduced, even when injecting a much higher cRNA amount per oocyte. Subsequent blue-light exposure of the oocytes failed to trigger typical ChR2 currents, suggesting that the ChR2 domain was not functional in both fusion proteins (Fig. 2 B). Because similar data were obtained in HEK293 cells (not depicted), we concluded that both fusion constructs cannot be functionally expressed in a heterologous host.

Coupling of ChR2 to the Na$^+$ channel β1 subunit

Next, we linked ChR2 to the C-terminus of the β1 subunit of voltage-gated Na$^+$ channels (Fig. 1). The specific interaction of this accessory subunit with its α subunit should direct the ChR2 moiety in close proximity to the Na$^+$ channel, thereby forming a light-sensitive channel complex: blue light–pulses should first activate ChR2, resulting in a small inward flux of positive ions. We hypothesized that the resulting slight membrane depolarization could be sufficient to exceed the threshold potential for voltage-gated Na$^+$ channels and thus to elicit an AP upstroke.

As a first step, we tested whether both β1 and ChR2 are functional in the fusion β1-ChR2. As shown in Fig. 3 A, blue light delivered to β1-ChR2–injected oocytes induced typical ChR2 inward currents. However, peak currents were significantly reduced from 6.09 ± 0.51 µA in ChR2 to 0.65 ± 0.07 µA in β1-ChR2 when injecting oocytes with 10 ng cRNA (Fig. 3 B). The ratio between peak and plateau current remained unchanged (see legend to Fig. 3). Similar data were obtained when coupling a second ChR2 to β1-ChR2. Using β1-ChR2-ChR2, we found peak current amplitudes of 0.65 ± 0.10 µA (Fig. 3 B).

To address the question of whether the observed current reduction was due to a reduced number of β1-ChR2 channels in the plasma membrane, we fused YFP to the C-terminus of β1-ChR2 and measured whole-cell fluorescence intensities using a
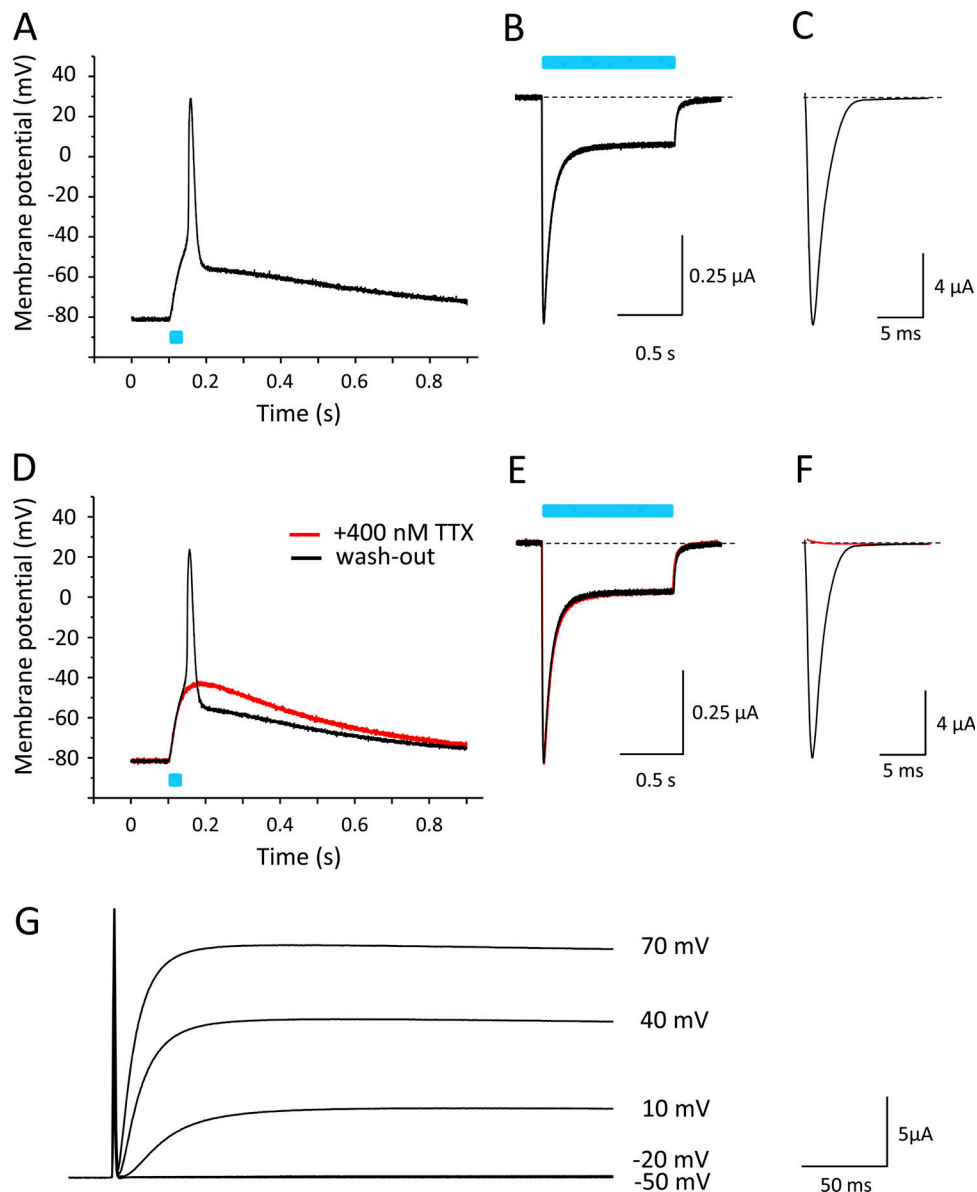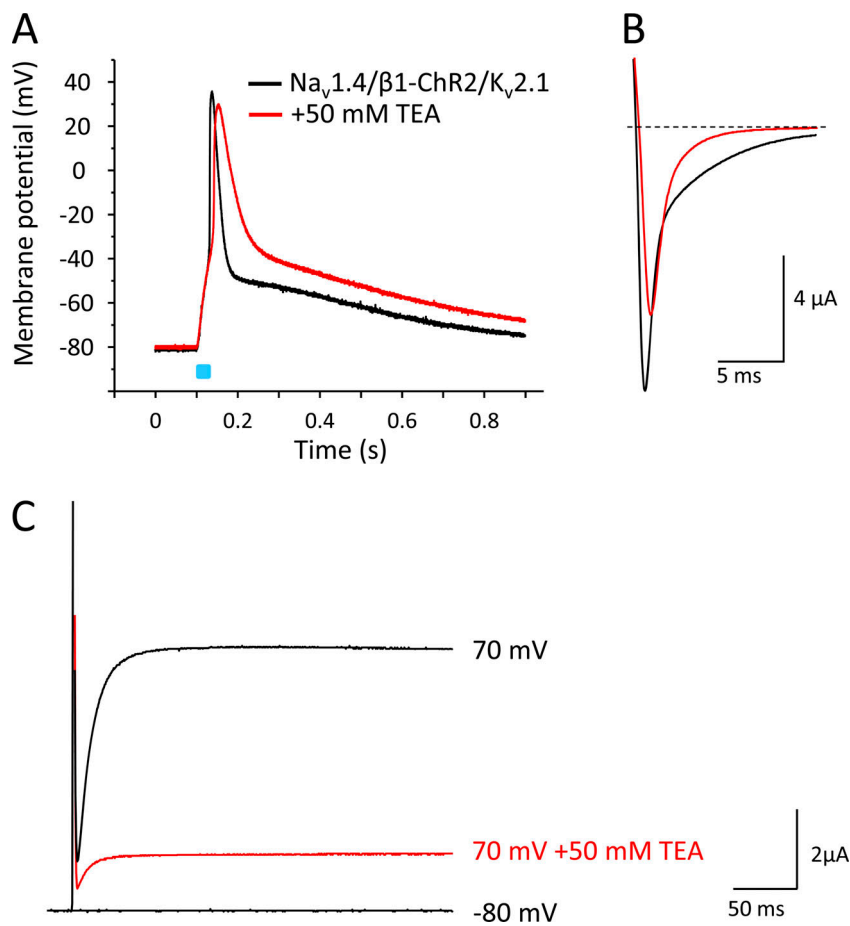
Figure 9. **Acceleration of AP repolarization by Kv2.1.** Recordings were performed on a single oocyte coexpressing Nav1.4, β1-ChR2, and Kv2.1. **(A)** Current-clamp recording (pulse duration 25 ms). For statistics on AP shortening by Kv2.1, see Table S1. **(B)** Corresponding whole-cell current through β1-ChR2 channels recorded in the voltage-clamp mode (pulse duration 1 s). **(C)** Nav1.4 whole-cell current of the same oocyte recorded in the voltage-clamp mode (test pulse −25 mV). **(D)** Current-clamp recording at 400 nM TTX (red). Washout restored the AP (black). **(E)** Currents through β1-ChR2 in the absence and presence of TTX (pulse duration 1 s). **(F)** Block of Nav1.4 channels by 400 nM TTX (red). Washout completely restored the voltage-gated Na+ current. **(G)** Corresponding Kv2.1 current (voltage-clamp mode). Test pulses are indicated. The overlapping Na+ current is not visible due to the presence of 400 nM TTX. The amount of coinjected Kv2.1 cRNA was 50 pg per oocyte. The magnitude of the injected current required to set the initial membrane potential to −80 mV was not altered by Kv2.1 coexpression.

laser scanning microscope (LSM710). The resulting β1-ChR2-YFP construct also contained a Golgi-to-plasma membrane trafficking signal (Hofherr et al., 2005) and the ER export motif FCYENEV (Stockklausner et al., 2001). Compared with oocytes injected with ChR2-YFP cRNA, fluorescence signals were markedly reduced in oocytes expressing β1-ChR2-YFP (see representative oocytes in Fig. 4 A). Surface fluorescence intensities determined by the implemented ZEN 2010 software were significantly decreased to 32.5% in β1-ChR2-YFP compared with ChR2-YFP (Fig. 4 B). Whole-cell photocurrents recorded in

parallel experiments were similarly reduced in β1-ChR2-YFP (31.9% versus ChR2-YFP; see Fig. 4, C and D). Taken together, these data suggest that the number of β1-ChR2 channels was reduced in the plasma membrane and that subcellular processing and trafficking of ChR2 was affected by coupling the Na+ channel β1 subunit. Photocurrents through β1-ChR2-YFP were larger compared with β1-ChR2 (1.94 ± 0.26 µA and 0.65 ± 0.07 µA, respectively; P < 0.05), suggesting that the trafficking and ER export signals in β1-ChR2-YFP enhanced cell surface expression.
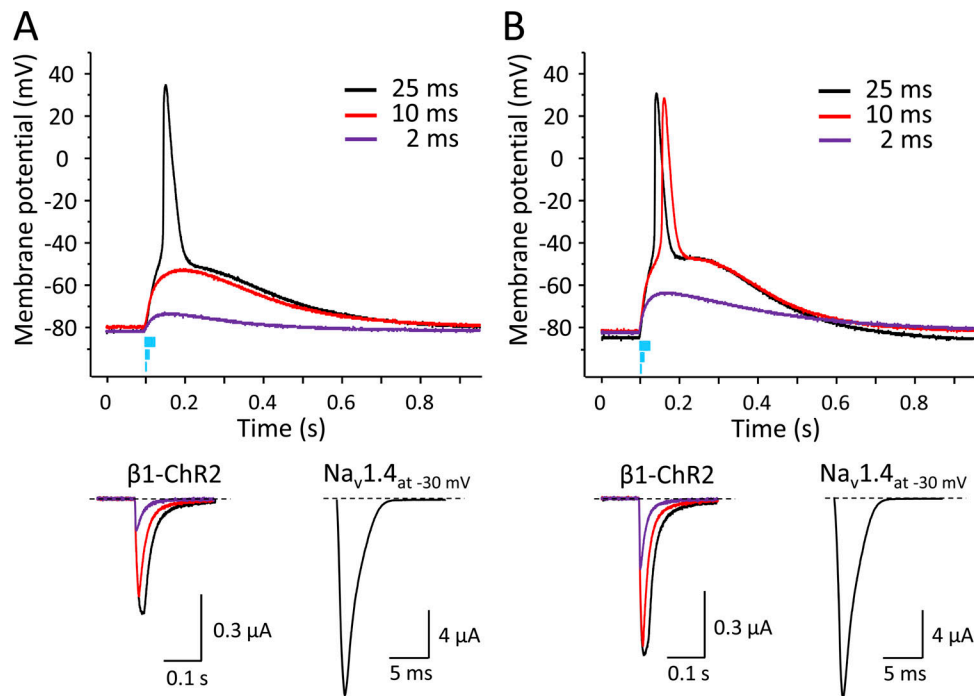
Figure 10. **Effect of the nonspecific K$^+$ channel blocker TEA on light-triggered APs in *Xenopus* oocytes.** Recordings were performed on a single oocyte expressing Na$_v$1.4, β1-ChR2, and K$_v$2.1. Duration of the light pulse was 25 ms. **(A)** Current-clamp recording in the absence and presence of 50 mM TEA. TEA reduced the upstroke velocity, which was due to a partial block of Na$_v$1.4 channels, and caused a deceleration of AP repolarization, which was due to a reduction of the K$_v$2.1 current. The early depolarization phase to nearly −55 mV remained unchanged, because β1-ChR2 currents were not affected by TEA. Corresponding light-triggered current values were as follows: I_{peak} = 581 ± 212 nA, $I_{plateau}$ = 279 ± 95 nA (without TEA), and I_{peak} = 605 ± 224 nA, $I_{plateau}$ = 307 ± 109 nA (50 mM TEA; P > 0.2 with n = 10). **(B)** Corresponding Na$_v$1.4 currents. The test pulse was −10 mV. At 50 mM TEA, Na$_v$1.4 was partially blocked (red). **(C)** Corresponding K$_v$2.1 currents. At 50 mM TEA, >75% of K$_v$2.1 channels were blocked, causing the pronounced AP prolongation seen in A.

Next, we coexpressed β1-ChR2 with the skeletal muscle isoform Na$_v$1.4 to test for functional interaction with a Na$^+$ channel α subunit. Modulatory effects of β1 can be easily followed by its ability to accelerate inactivation of brain-type and skeletal muscle Na$^+$ channels in *Xenopus* oocytes (Isom et al., 1992; Wallner et al., 1993; Patton et al., 1994; Chen and Cannon, 1995). In mammalian cell systems, this β1 effect cannot be observed, i.e., expression of α subunits alone is sufficient to record fast-inactivating Na$^+$ currents (Ukomadu et al., 1992; West et al., 1992). As shown in Fig. 5 (red lines), expression of Na$_v$1.4 resulted in the typical slow decay of macroscopic whole-cell currents. When coexpressing β1, inactivation of Na$_v$1.4 was significantly accelerated. Both the fast and slow time constants of inactivation, τ_f and τ_s, were significantly shortened (see values in Fig. 5). This specific β1 property was also intrinsic to both β1-ChR2 and β1-ChR2-ChR2, suggesting that ChR2 linkage did not alter important structural and functional β1 features. Moreover, we determined a variety of kinetic parameters of Na$_v$1.4 channels in the absence and presence of one of the three β1 constructs. We found (1) that steady-state activation and inactivation were shifted toward hyperpolarized potentials (Table 1), and (2) that recovery from inactivation was faster when coexpressing either wild type β1 or one of the β1-linked ChR2 variants (Fig. 6 and Table 1). Coexpression of ChR2 alone had no effect on Na$^+$ channel properties (Figs. 5 and 6 and Table 1).

In conclusion, expression of β1-ChR2 and β1-ChR2-ChR2 resulted in both typical ChR2 currents and β1-modulatory effects on Na$_v$1.4. Because we could not observe a difference between the two fusions, we continued with β1-ChR2.

Light-induced APs using the ChR2-linked β1 subunit and Na$_v$1.4
After confirming that ChR2 coupling did not affect modulatory functions of the β1 subunit, we injected oocytes with cRNA for Na$_v$1.4 and β1-ChR2 at an equimolar ratio (10 and 2.75 ng per oocyte, respectively). We recorded light-induced voltage changes in the current-clamp mode after an incubation time of 3 d (Fig. 7). As shown in Fig. 7 A, a 25-ms blue-light pulse caused a rapid change of membrane voltage, resembling the steep upstroke of a typical AP of excitable cells. The fast upstroke from −80 mV to nearly +20 mV was followed by a long repolarization phase. Voltage-clamp recordings confirmed the expression of β1-ChR2 and Na$_v$1.4 (Fig. 7, B and C, respectively). To confirm that the rapid depolarization phase was due to Na$^+$ channel activity, we applied 400 nM of the highly specific Na$^+$ channel blocker TTX. As shown in Fig. 7 D, the 25-ms light pulse did not result in an overshoot to positive membrane potentials (red line). Currents through β1-ChR2 were not affected (Fig. 7 E), indicating that the initial depolarization to approximately −35 mV in the presence of TTX was due to ChR2 activity. The following fast upstroke to positive potentials, illustrated in Fig. 7 A, can be clearly attributed to Na$_v$1.4 activity, because the toxin completely

Walther et al.
Light-induced action potentials in *Xenopus* oocytes

Journal of General Physiology
https://doi.org/10.1085/jgp.201912489

10 of 16

Figure 11. **Effect of light pulse duration in two different oocytes coexpressing Na$_v$1.4, β1-ChR2, and K$_v$2.1 on the membrane potential and on the corresponding photocurrent.** Duration of the light flashes was 25, 10, and 2 ms. Amounts of coinjected cRNA per oocyte were 10 ng Na$_v$1.4, 2.75 ng β1-ChR2, and 50 pg K$_v$2.1. **(A)** The 25-ms pulse induced a peak photocurrent of 0.51 μA, which led to successful AP triggering in this oocyte (black line). In contrast, 10 and 2 ms were too short to activate a sufficient number of β1-ChR2 channels, so the threshold potential was not achieved (red and purple lines, respectively). Light-induced peak currents were 0.44 and 0.14 μA, respectively. **(B)** Blue-light pulses induced larger photocurrents, indicating a higher β1-ChR2 expression level. The 25-ms pulse resulted in a peak photocurrent of 0.70 μA and produced a typical AP (black). The short 2-ms pulse was not sufficient to elicit an AP. The corresponding light-induced current of 0.31 μA was larger than in A, and consequently, the subthreshold depolarization was more pronounced (compare purple curves in upper graphs in A and B). Application of an intermediate pulse (10 ms, red) resulted in a peak photocurrent of 0.67 μA, and in above-threshold activation. However, depolarization was delayed compared with the longer light pulse of 25 ms. In both oocytes, the membrane resistance as well as the Na$_v$1.4 current at −30 mV were very similar (0.59 MΩ and 16.6 μA in A and 0.5 MΩ and 16.9 μA in B, respectively). K$^+$ currents at +70 mV were 6.4 μA (A) and 8.0 μA (B).

blocked voltage-gated Na$^+$ currents at 400 nM (red line in Fig. 7 F). Washout of TTX restored both the light-triggered AP and Na$_v$1.4 currents (black lines in Fig. 7, D and F, respectively).

In Fig. 8 A, the light-induced current was plotted under the AP of another oocyte coexpressing Na$_v$1.4 and β1-ChR2. At a holding potential of −80 mV, the short light pulse caused an inward current through β1-ChR2. Corresponding changes of the membrane voltage toward depolarized potentials should be rapidly corrected by the amplifier, owing to its fast clamp properties. Consequently, Na$^+$ currents through Na$_v$1.4 are not possible when clamping the membrane voltage at −80 mV, and application of 400 nM TTX did not result in a current reduction (Fig. 8 B). At the same time, blocking of Na$_v$1.4 channels did not lead to a reversion of the membrane polarity, similarly as shown in Fig. 7. As further shown in Figs. 7 and 8, repolarization was extremely long. The oocyte membrane remained depolarized usually for >1 s. Voltage-gated Na$^+$ channels are inactivated within a few milliseconds, and currents through β1-ChR2 can at most partially account for a prolonged repolarization, because this channel also rapidly inactivates in the dark (see Fig. 8). Even at a membrane potential of −80 mV, β1-ChR2 currents drop to <5% of the transient current after ~100 ms, and channels were

fully closed or inactivated after ~300 ms. The long repolarization phase must largely depend on endogenous channels activated during β1-ChR2-/Na$_v$1.4-mediated depolarization, as discussed later.

AP shortening by K$_v$2.1 coexpression

To facilitate AP repolarization, we coexpressed in addition to Na$_v$1.4 and β1-ChR2 the delayed rectifier K$^+$ channel K$_v$2.1. We assumed that this channel should be activated during the depolarization phase, as similarly observed in native excitable cells. As illustrated for a representative oocyte in Fig. 9 A, the K$^+$ channel clearly accelerated repolarization. Membrane potentials changed from approximately +30 mV to −60 mV within <30 ms. Thus, repolarization in the presence of K$_v$2.1 occurred similarly as fast as depolarization. Similarly, as shown in Fig. 7, the overshoot of the AP and the inward current through Na$_v$1.4 channels were absent when applying TTX (Fig. 9, D and F, respectively). The toxin had no effect on β1-ChR2 currents (Fig. 9 E). The corresponding K$^+$ currents through K$_v$2.1 are illustrated in Fig. 9 G.

To better illustrate the effect of K$_v$2.1 on AP repolarization, we applied the nonspecific K$^+$ channel blocker TEA (50 mM; Fig. 10). Using this compound, we noticed two effects. First,
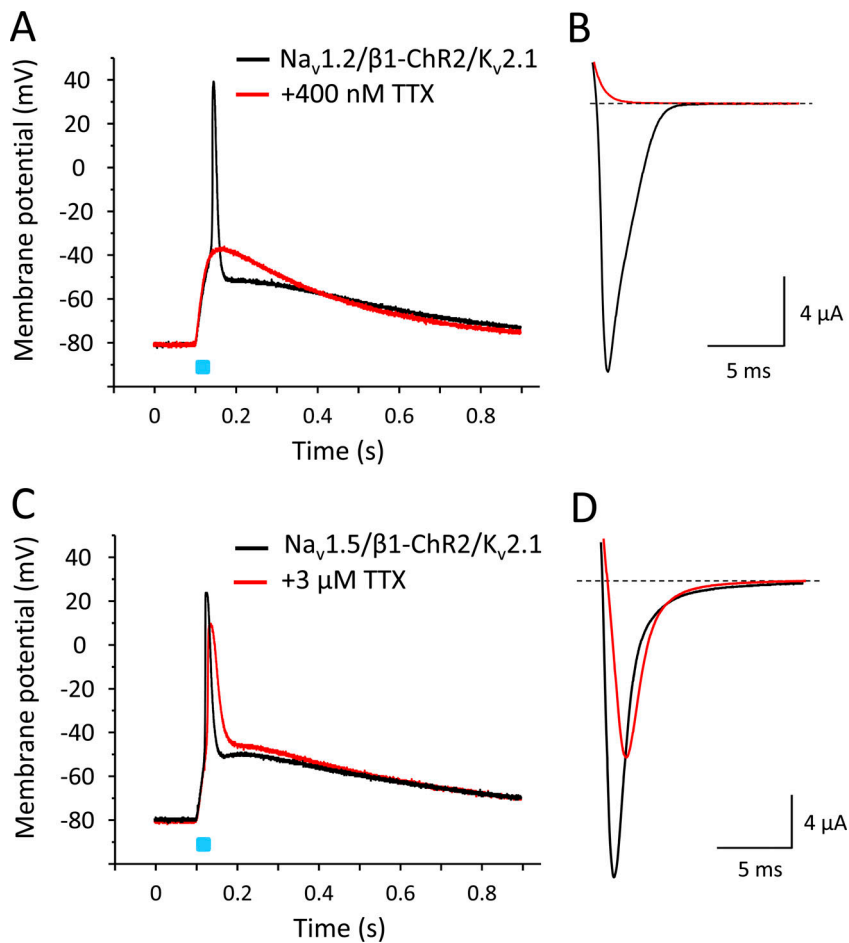
Figure 12. **Light-induced APs in *Xenopus* oocytes coexpressing β1-ChR2 and K$_v$2.1 with either Na$_v$1.2 or Na$_v$1.5. (A and C)** Current-clamp recordings. For detailed statistics on the effect of K$_v$2.1 on Na$_v$1.5-mediated APs, see Fig. S2 and Table S2. **(B and D)** Corresponding Na$^+$ currents in the absence and presence of TTX. Similarly to Na$_v$1.4, neuronal Na$_v$1.2 channels belong to the TTX-sensitive Na$^+$ channels; they can be blocked at nanomolar TTX concentrations. Cardiac Na$_v$1.5 channels are TTX resistant, with IC$_{50}$ values >1 μM. The peak and plateau currents through β1-ChR2 were I_{peak} = 768 nA, $I_{plateau}$ = 193 nA (Na$_v$1.2-expressing cell in A and B), and I_{peak} = 957 nA, $I_{plateau}$ = 193 nA (Na$_v$1.5-expressing cell in C and D). The K$^+$ currents through K$_v$2.1 were $I_{+70\ mV}$ = 14.3 μA (Na$_v$1.2-expressing cell, A and B), and $I_{+70\ mV}$ = 30.9 μA (Na$_v$1.5-expressing cell, C and D). Duration of the light pulse was 25 ms.

repolarization was clearly delayed when >75% of K$_v$2.1 channels were blocked at this TEA concentration (red lines in Fig. 10, A and C). Second, AP upstroke velocity was slightly reduced, which was due to a partial block of Na$_v$1.4 channels (Fig. 10 B; O'Leary and Horn, 1994). TEA did not affect β1-ChR2 currents (see current data in legend to Fig. 10). Correspondingly, we did not observe an alteration of the early depolarization phase (Fig. 10 A).

In conclusion, the channel combination Na$_v$1.4/β1-ChR2/K$_v$2.1 can be used to generate light-induced fast alterations of membrane voltage, strongly resembling typical APs of excitable cells. However, complete repolarization to the resting potential lasted for ~1 s also in the presence of the delayed rectifier K$_v$2.1. We therefore applied shorter light pulses to estimate the threshold photocurrent and answer the question of whether the long-lasting post-spike depolarization could be limited when fewer β1-ChR2 channels are activated. Fig. 11 shows the effect of the light pulse duration on both the membrane potential and the corresponding photocurrent for two different oocytes coexpressing Na$_v$1.4, β1-ChR2, and K$_v$2.1 (Fig. 11, A and B). Application of blue light for 25 ms resulted in typical APs in both oocytes (black lines in Fig. 11, A and B, upper part). The corresponding β1-ChR2 currents were 0.51 and 0.70 μA, respectively. In both cases, however, the 2-ms light pulse was not sufficient to trigger APs (purple lines in Fig. 11, A and B, upper part). The corresponding β1-ChR2 currents were 0.14 and 0.31 μA, respectively. The intermediate pulse duration of 10 ms resulted in a differential

effect. In one oocyte, the induced photocurrent of 0.44 μA was not sufficient to elicit an AP (red lines in Fig. 11 A). In the second oocyte, the 10-ms flash produced an above-threshold photocurrent of 0.67 μA (red lines in Fig. 11 B). Compared with the corresponding 25-ms pulse, however, the AP upstroke was slightly delayed. In conclusion, APs could be obtained using this batch of oocytes, when the light-induced photocurrent through β1-ChR2 channels and the Na$_v$1.4 currents were ≥0.51 and 16.6 μA, respectively. Both conditions are fulfilled at 25 ms in Fig. 11 A as well as at 10 ms in Fig. 11 B. Moreover, the shorter light pulse of 10 ms did not substantially affect the long-lasting cell depolarization phase, independently of whether an AP was induced (compare red and black lines in Fig. 11, A and B).

Light-induced APs using brain- and heart-type Na$^+$ channels
Because the β1 subunit is widely expressed in excitable tissues and interacts with various Na$^+$ channels, we tested whether APs can be also triggered when coexpressing neuronal Na$_v$1.2 and cardiac Na$_v$1.5 channels with β1-ChR2. To facilitate repolarization, we also coinjected cRNA for K$_v$2.1. As shown in Fig. 12, both Na$^+$ channels caused a fast alteration of the membrane potential, similarly as observed for the skeletal muscle isoform Na$_v$1.4. In case of neuronal Na$_v$1.2, application of 400 nM TTX completely blocked the Na$^+$ inward current, and consequently, also the light-induced overshoot to positive potentials (Fig. 12, A and B). In contrast to Na$_v$1.2, the cardiac Na$^+$ channel Na$_v$1.5 belongs to
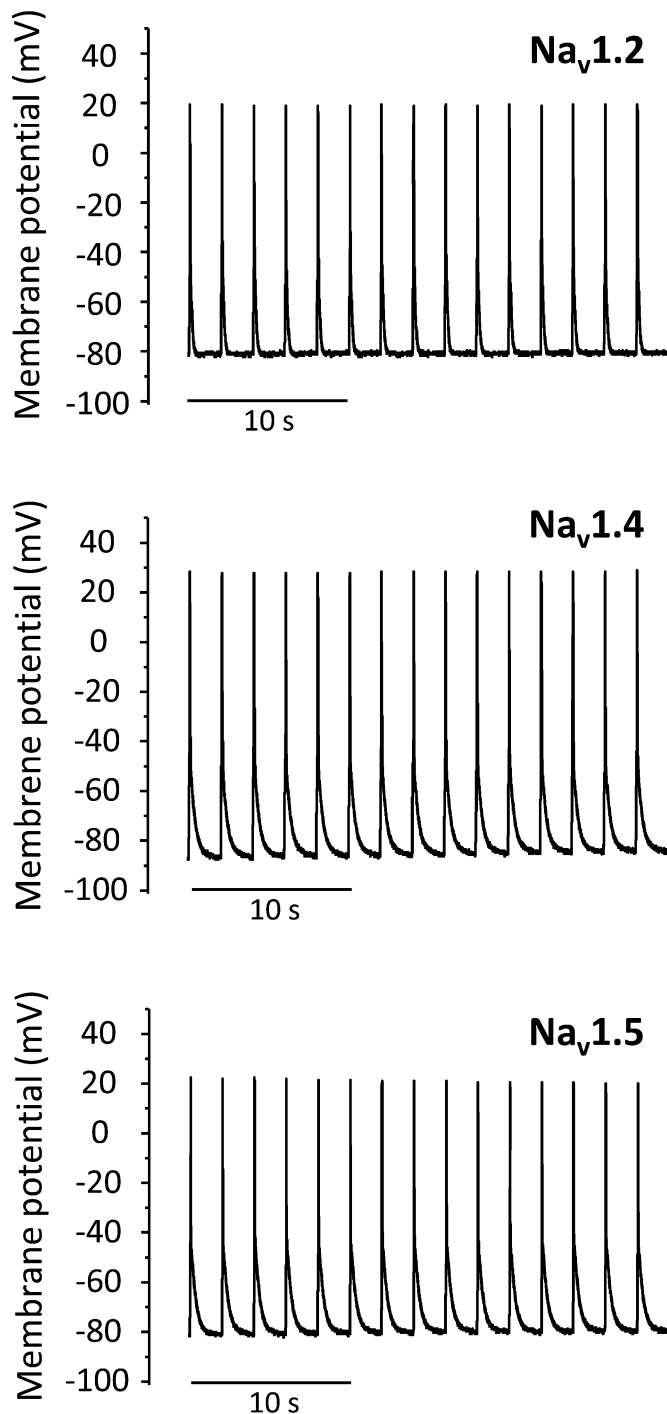
Figure 13.   **Repetitive firing of light-triggered APs in *Xenopus* oocytes coexpressing either neuronal Na$_v$1.2, skeletal muscle Na$_v$1.4, or cardiac Na$_v$1.5 with β1-ChR2 and K$_v$2.1.** The membrane potential was set to –80 mV (Na$_v$1.2 or Na$_v$1.5) or –85 mV (Na$_v$1.4), and the change of membrane voltage was followed in the current-clamp mode on 50-ms light pulses every 2 s.

Finally, we tested whether APs can be obtained repetitively. We applied 50-ms light pulses every 2 s to whole oocytes co-expressing Na$_v$1.2, Na$_v$1.4, or Na$_v$1.5 with β1-ChR2 and K$_v$2.1. Fig. 13 illustrates that AP firing at 0.5 Hz could be triggered with all three Na$^+$ channel subtypes.

Discussion

In the present study, we provide a novel optogenetic tool to switch naturally nonexcitable cells into excitable cells and to study the shape of APs. Using a fusion construct consisting of ChR2 and the common β1 subunit of voltage-gated Na$^+$ channels, we were able to elicit APs in *Xenopus* oocytes expressing neuronal, skeletal muscle, or cardiac voltage-gated Na$^+$ channels.

Recently, Corbin-Leftwich et al. also recorded APs in the same expression system using a set of ion channels, including Na$_v$1.4/β1 and non–voltage-gated and voltage-gated K$^+$ channels (Corbin-Leftwich et al., 2016, 2018). In contrast to our study, the authors adapted the voltage-clamping circuits of a traditional two-electrode voltage-clamp setup, so that fast changes of membrane voltage became visible ("loose-clamp" mode). Besides current injection and light activation, there are more possibilities to elicit APs. Shapiro et al. (2012) discovered the opto-capacitance mechanism, in which infrared radiation increases membrane temperature and its capacitance. The capacitor discharge leads to a current that is sufficient to generate APs (Shapiro et al., 2012; Carvalho-de-Souza et al., 2018). Furthermore, other studies have shown the transformation of non-excitable HEK293 cells into spontaneously firing cells by overexpressing voltage-gated Na$^+$ channels and inward rectifier K$^+$ channels (Park et al., 2013; McNamara et al., 2016; Ling et al., 2018). Moreover, coexpression of the channelrhodopsin variant CheRiff in these spiking HEK293 cells even allowed for blue-light controlled AP firing (Hochbaum et al., 2014; McNamara et al., 2016).

We have chosen the major β subunit of voltage-gated Na$^+$ channels for an optogenetic AP firing because of the following reasons. First, the β1 subunit interacts with various voltage-gated Na$^+$ channels. Consequently, β1-ChR2 fusions could be used as optical switches for several Na$^+$ channel isoforms in different excitable tissues. Second, neuronal, skeletal muscle, and cardiac Na$^+$ channels even require coexpression of β1 for normal channel gating. Consequently, coexpression of β1-coupled ChR2 channels in normally nonexcitable cells should result in native Na$^+$ currents and in an AP upstroke velocity more closely resembling the in vivo situation. For example, the shift of steady-state activation toward hyperpolarized potentials should facilitate AP spiking, thereby compensating for a lower expression of β1-ChR2.

There are several potential applications for this novel optogenetic tool. First, one could address basic questions regarding the effect of individual ion fluxes on AP shape, similarly as reported recently (Corbin-Leftwich et al., 2018). For example, it seems to be promising to include naturally occurring mutations causing life-threatening channelopathies such as epilepsy, Brugada syndrome, sick sinus syndrome, or long QT syndrome (Webster and Berul, 2013). Hundreds of monogenetic long QT

the TTX-resistant Na$^+$ channels, with reported IC$_{50}$ values ≤6 µM (Goldin, 2001). Application of 3 µM TTX blocked <50% of Na$_v$1.5 channels (Fig. 12 D). The remaining channels were sufficient to trigger an AP-like alteration of the membrane potential. At the same time, we noticed a reduced AP upstroke velocity and amplitude.

syndrome variations are known to cause electrocardiogram alterations and sudden cardiac death (Zimmer and Surber, 2008; Bohnen et al., 2017), but very limited data are available regarding the actual impact of a given point mutation on AP shape. The challenging possibility to specifically design APs could be the basis for a second application, a drug screening of host cells expressing wild type or mutant channels associated with epilepsy or cardiac events. It would be conceivable, and should be possible, even to develop respective high-throughput systems with blue LEDs. Third, β1-ChR2 could be expressed not only in heterologous cells such as *Xenopus* oocytes or HEK293 cells, but also in neurons, cardiomyocytes, or other mammalian cells, either using suitable in vitro transfection methods or transgenic animal technologies. It is possible that, in contrast to wild type ChR2, β1-ChR2 will preferentially localize at cellular spots with a high density of native Na+ channels so that light-induced APs originate more specifically at the physiological site, such as the axon hillock or the intercalated disc region.

Despite our enthusiasm, we have to be sensitive to all the present limitations. First of all, our β1-ChR2 construct seems not to be optimal, considering the reduction in surface expression and light-induced ChR2 currents (see Figs. 3 and 4). Surprisingly, coupling a second ChR2 did not help, suggesting either that one of the ChR2 channel domains in β1-ChR2-ChR2 is inactive, or that intracellular processing is less efficient and/or that degradation is enhanced. Interestingly, we recorded larger photocurrents in β1-ChR2-YFP compared with β1-ChR2 (Figs. 3 B and 4 D). The reason for a higher expression level of the YFP-coupled variant is actually unknown. We suggest that incorporation of established trafficking and ER export signals (Stockklausner et al., 2001; Hofherr et al., 2005), which are present in β1-ChR2-YFP, are a first promising option to improve β1-ChR2 and β1-ChR2-ChR2. Second, ChR2 also conducts Ca2+, which might in turn affect intracellular pathways or endogenous ion channels of the host cell. Future studies using Ca2+-free solution or ChR2 mutants with a reduced Ca2+ conductance (Cho et al., 2019) may eliminate or reduce possible secondary Ca2+ effects. Third, to elicit an AP, three major conditions must be met: (1) a sufficient photocurrent, (2) a high density of Na+ channels, and (3) a high resistance of the oocyte membrane. If one of those parameters is suboptimal, others could compensate. For example, even equimolar Na$_v$1.4 and β1-ChR2 cRNA ratios did not result in constant Na$_v$1.4 and β1-ChR2 current ratios, and APs could be triggered at lower Na+ and higher ChR2 currents and vice versa (see Table S1 and Table S2). Future studies with defined TTX concentrations and varying light intensities could be helpful to adjust a constant Na+ to β1-ChR2 channel ratio, so that AP initiation can be more exactly controlled. Currently, we can adjust cRNA ratios, define a cutoff for the membrane resistance (see Materials and methods), and show AP variability and statistics on threshold, overshoot, rise time, and duration (see Table S1 and Table S2). However, it is difficult to exactly control the size of voltage- and light-activated currents as well as the membrane resistance.

Fourth, *Xenopus* oocytes express a variety of endogenous channels activated by depolarization, hyperpolarization, mechanical stress, and various chemicals or ligands (Weber, 1999;

Terhag et al., 2010). The pronounced repolarization phase observed upon Na$_v$1.4/β1-ChR2 coexpression (Figs. 7 and 8) should be largely the result of an endogenous current ensemble. This assumption is supported by our observation that the shape and duration of the repolarization phase varied between the oocyte batches. Moreover, when comparing the time scale of the long-lasting repolarization with the light-induced inward current (Fig. 8 A), it can be suggested that direct depolarizing effects of Na$_v$1.4 and β1-ChR2 on this later AP phase are negligibly low. Candidates contributing to a delayed cell repolarization are voltage-dependent Ca2+ and Ca2+-activated Cl− channels (Barish, 1983; Weber, 1999; Caldwell et al., 2008; Terhag et al., 2010; Corbin-Leftwich et al., 2018). Both may counteract the simultaneous K+ outward flux. Corbin-Leftwich et al. (2018) discussed the impact of the Ca2+-activated Cl− channels in oocytes and showed that a reduced external Cl− concentration prolongs the repolarization phase. Caldwell et al. (2008) used this endogenous current to monitor the intracellular Ca2+ level to show that mGluR7 signaling is potentiated by a physiological Ca2+ concentration. Currently, this long repolarization is the major limiting factor for repetitive AP firing. Even when coexpressing K$_v$2.1, we rarely obtained frequencies >0.5 Hz (see Fig. 13). This delayed rectifier K+ channel caused a rapid repolarization up to −55 mV (Figs. 9, 10, 11, and 12). However, full recovery of voltage-gated Na+ channels cannot be achieved at such membrane potentials (see values for steady-state inactivation in Table 1). Our ongoing research with other K+ channel subtypes and measurements in Ca2+-free solutions may further accelerate the AP downstroke, leading to higher AP frequencies. Moreover, it is not unlikely that membrane repolarization is significantly faster when expressing β1-ChR2 in cardiomyocytes or neurons.

In conclusion, β1-ChR2 in combination with a voltage-gated K+ channel is a useful tool to generate light-induced APs with a variety of voltage-gated Na+ channels in naturally unexcitable cells. We are optimistic that current limitations can be overcome and that the new β1-ChR2 fusion construct can promote research in optogenetics.

Acknowledgments

References

Auld, V.J., A.L. Goldin, D.S. Krafte, J. Marshall, J.M. Dunn, W.A. Catterall, H.A. Lester, N. Davidson, and R.J. Dunn. 1988. A rat brain Na+ channel alpha subunit with novel gating properties. *Neuron.* 1:449–461. https://doi.org/10.1016/0896-6273(88)90176-6

Barish, M.E. 1983. A transient calcium-dependent chloride current in the immature Xenopus oocyte. *J. Physiol.* 342:309–325. https://doi.org/10.1113/jphysiol.1983.sp014852

Berndt, A., P. Schoenenberger, J. Mattis, K.M. Tye, K. Deisseroth, P. Hegemann, and T.G. Oertner. 2011. High-efficiency channelrhodopsins for fast neuronal stimulation at low light levels. *Proc. Natl. Acad. Sci. USA.* 108:7595–7600. https://doi.org/10.1073/pnas.1017210108

Bezanilla, F. 1987. Single sodium channels from the squid giant axon. *Biophys. J.* 52:1087–1090. https://doi.org/10.1016/S0006-3495(87)83304-0

Bi, A., J. Cui, Y.P. Ma, E. Olshevskaya, M. Pu, A.M. Dizhoor, and Z.H. Pan. 2006. Ectopic expression of a microbial-type rhodopsin restores visual responses in mice with photoreceptor degeneration. *Neuron.* 50:23–33. https://doi.org/10.1016/j.neuron.2006.02.026

Bohnen, M.S., G. Peng, S.H. Robey, C. Terrenoire, V. Iyer, K.J. Sampson, and R.S. Kass. 2017. Molecular Pathophysiology of Congenital Long QT Syndrome. *Physiol. Rev.* 97:89–134. https://doi.org/10.1152/physrev.00008.2016

Boyden, E.S., F. Zhang, E. Bamberg, G. Nagel, and K. Deisseroth. 2005. Millisecond-timescale, genetically targeted optical control of neural activity. *Nat. Neurosci.* 8:1263–1268. https://doi.org/10.1038/nn1525

Brackenbury, W.J., and L.L. Isom. 2011. Na Channel β Subunits: Overachievers of the Ion Channel Family. *Front. Pharmacol.* 2:53. https://doi.org/10.3389/fphar.2011.00053

Caldwell, J.H., G.A. Herin, G. Nagel, E. Bamberg, A. Scheschonka, and H. Betz. 2008. Increases in intracellular calcium triggered by channelrhodopsin-2 potentiate the response of metabotropic glutamate receptor mGluR7. *J. Biol. Chem.* 283:24300–24307. https://doi.org/10.1074/jbc.M802593200

Carvalho-de-Souza, J.L., B.I. Pinto, D.R. Pepperberg, and F. Bezanilla. 2018. Optocapacitive Generation of Action Potentials by Microsecond Laser Pulses of Nanojoule Energy. *Biophys. J.* 114:283–288. https://doi.org/10.1016/j.bpj.2017.11.018

Catterall, W.A. 2017. Forty Years of Sodium Channels: Structure, Function, Pharmacology, and Epilepsy. *Neurochem. Res.* 42:2495–2504. https://doi.org/10.1007/s11064-017-2314-9

Chen, C., and S.C. Cannon. 1995. Modulation of Na+ channel inactivation by the beta 1 subunit: a deletion analysis. *Pflugers Arch.* 431:186–195. https://doi.org/10.1007/BF00410190

Cho, Y.K., D. Park, A. Yang, F. Chen, A.S. Chuong, N.C. Klapoetke, and E.S. Boyden. 2019. Multidimensional screening yields channelrhodopsin variants having improved photocurrent and order-of-magnitude reductions in calcium and proton currents. *J. Biol. Chem.* 294:3806–3821. https://doi.org/10.1074/jbc.RA118.006996

Corbin-Leftwich, A., S.M. Mossadeq, J. Ha, I. Ruchala, A.H. Le, and C.A. Villalba-Galea. 2016. Retigabine holds KV7 channels open and stabilizes the resting potential. *J. Gen. Physiol.* 147:229–241. https://doi.org/10.1085/jgp.201511517

Corbin-Leftwich, A., H.E. Small, H.H. Robinson, C.A. Villalba-Galea, and L.M. Boland. 2018. A *Xenopus* oocyte model system to study action potentials. *J. Gen. Physiol.* 150:1583–1593. https://doi.org/10.1085/jgp.201812146

Deisseroth, K., and P. Hegemann. 2017. The form and function of channelrhodopsin. *Science.* 357:eaan5544. https://doi.org/10.1126/science.aan5544

Feldbauer, K., D. Zimmermann, V. Pintschovius, J. Spitz, C. Bamann, and E. Bamberg. 2009. Channelrhodopsin-2 is a leaky proton pump. *Proc. Natl. Acad. Sci. USA.* 106:12317–12322. https://doi.org/10.1073/pnas.0905852106

Gellens, M.E., A.L. George Jr., L.Q. Chen, M. Chahine, R. Horn, R.L. Barchi, and R.G. Kallen. 1992. Primary structure and functional expression of the human cardiac tetrodotoxin-insensitive voltage-dependent sodium channel. *Proc. Natl. Acad. Sci. USA.* 89:554–558. https://doi.org/10.1073/pnas.89.2.554

Goldin, A.L. 2001. Resurgence of sodium channel research. *Annu. Rev. Physiol.* 63:871–894. https://doi.org/10.1146/annurev.physiol.63.1.871

Goldin, A.L., R.L. Barchi, J.H. Caldwell, F. Hofmann, J.R. Howe, J.C. Hunter, R.G. Kallen, G. Mandel, M.H. Meisler, Y.B. Netter, et al. 2000.

Nomenclature of voltage-gated sodium channels. *Neuron.* 28:365–368. https://doi.org/10.1016/S0896-6273(00)00116-1

Gütter, C., K. Benndorf, and T. Zimmer. 2013. Characterization of N-terminally mutated cardiac Na(+) channels associated with long QT syndrome 3 and Brugada syndrome. *Front. Physiol.* 4:153. https://doi.org/10.3389/fphys.2013.00153

Hochbaum, D.R., Y. Zhao, S.L. Farhi, N. Klapoetke, C.A. Werley, V. Kapoor, P. Zou, J.M. Kralj, D. Maclaurin, N. Smedemark-Margulies, et al. 2014. All-optical electrophysiology in mammalian neurons using engineered microbial rhodopsins. *Nat. Methods.* 11:825–833. https://doi.org/10.1038/nmeth.3000

Hofherr, A., B. Fakler, and N. Klöcker. 2005. Selective Golgi export of Kir2.1 controls the stoichiometry of functional Kir2.x channel heteromers. *J. Cell Sci.* 118:1935–1943. https://doi.org/10.1242/jcs.02322

Ishizuka, T., M. Kakuda, R. Araki, and H. Yawo. 2006. Kinetic evaluation of photosensitivity in genetically engineered neurons expressing green algae light-gated channels. *Neurosci. Res.* 54:85–94. https://doi.org/10.1016/j.neures.2005.10.009

Isom, L.L., K.S. De Jongh, D.E. Patton, B.F. Reber, J. Offord, H. Charbonneau, K. Walsh, A.L. Goldin, and W.A. Catterall. 1992. Primary structure and functional expression of the beta 1 subunit of the rat brain sodium channel. *Science.* 256:839–842. https://doi.org/10.1126/science.1375395

Kleinlogel, S., U. Terpitz, B. Legrum, D. Gökbuget, E.S. Boyden, C. Bamann, P.G. Wood, and E. Bamberg. 2011. A gene-fusion strategy for stoichiometric and co-localized expression of light-gated membrane proteins. *Nat. Methods.* 8:1083–1088. https://doi.org/10.1038/nmeth.1766

Koopmann, R., A. Scholle, J. Ludwig, T. Leicher, T. Zimmer, O. Pongs, and K. Benndorf. 2001. Role of the S2 and S3 segment in determining the activation kinetics in Kv2.1 channels. *J. Membr. Biol.* 182:49–59. https://doi.org/10.1007/s00232-001-0029-X

Li, X., D.V. Gutierrez, M.G. Hanson, J. Han, M.D. Mark, H. Chiel, P. Hegemann, L.T. Landmesser, and S. Herlitze. 2005. Fast noninvasive activation and inhibition of neural and network activity by vertebrate rhodopsin and green algae channelrhodopsin. *Proc. Natl. Acad. Sci. USA.* 102:17816–17821. https://doi.org/10.1073/pnas.0509030102

Ling, T., K.C. Boyle, G. Goetz, P. Zhou, Y. Quan, F.S. Alfonso, T.W. Huang, and D. Palanker. 2018. Full-field interferometric imaging of propagating action potentials. *Light Sci. Appl.* 7:107. https://doi.org/10.1038/s41377-018-0107-9

McNamara, H.M., H.K. Zhang, C.A. Werley, and A.E. Cohen. 2016. Optically Controlled Oscillators in an Engineered Bioelectric Tissue. *Phys. Rev. X.* 6:031001.

Nagel, G., M. Brauner, J.F. Liewald, N. Adeishvili, E. Bamberg, and A. Gottschalk. 2005. Light activation of channelrhodopsin-2 in excitable cells of Caenorhabditis elegans triggers rapid behavioral responses. *Curr. Biol.* 15:2279–2284. https://doi.org/10.1016/j.cub.2005.11.032

Nagel, G., D. Ollig, M. Fuhrmann, S. Kateriya, A.M. Musti, E. Bamberg, and P. Hegemann. 2002. Channelrhodopsin-1: a light-gated proton channel in green algae. *Science.* 296:2395–2398. https://doi.org/10.1126/science.1072068

Nagel, G., T. Szellas, W. Huhn, S. Kateriya, N. Adeishvili, P. Berthold, D. Ollig, P. Hegemann, and E. Bamberg. 2003. Channelrhodopsin-2, a directly light-gated cation-selective membrane channel. *Proc. Natl. Acad. Sci. USA.* 100:13940–13945. https://doi.org/10.1073/pnas.1936192100

Nuss, H.B., N. Chiamvimonvat, M.T. Pérez-García, G.F. Tomaselli, and E. Marbán. 1995. Functional association of the beta 1 subunit with human cardiac (hH1) and rat skeletal muscle (mu 1) sodium channel alpha subunits expressed in Xenopus oocytes. *J. Gen. Physiol.* 106:1171–1191. https://doi.org/10.1085/jgp.106.6.1171

O'Leary, M.E., and R. Horn. 1994. Internal block of human heart sodium channels by symmetrical tetra-alkylammoniums. *J. Gen. Physiol.* 104:507–522. https://doi.org/10.1085/jgp.104.3.507

Park, J., C.A. Werley, V. Venkatachalam, J.M. Kralj, S.D. Dib-Hajj, S.G. Waxman, and A.E. Cohen. 2013. Screening fluorescent voltage indicators with spontaneously spiking HEK cells. *PLoS One.* 8:e85221. https://doi.org/10.1371/journal.pone.0085221

Patton, D.E., L.L. Isom, W.A. Catterall, and A.L. Goldin. 1994. The adult rat brain beta 1 subunit modifies activation and inactivation gating of multiple sodium channel alpha subunits. *J. Biol. Chem.* 269:17649–17655.

Schneider, F., C. Grimm, and P. Hegemann. 2015. Biophysics of Channelrhodopsin. *Annu. Rev. Biophys.* 44:167–186. https://doi.org/10.1146/annurev-biophys-060414-034014

Shapiro, M.G., K. Homma, S. Villarreal, C.P. Richter, and F. Bezanilla. 2012. Infrared light excites cells by changing their electrical capacitance. *Nat. Commun.* 3:736. https://doi.org/10.1038/ncomms1742

Sigworth, F.J., and E. Neher. 1980. Single Na+ channel currents observed in cultured rat muscle cells. *Nature.* 287:447–449. https://doi.org/10.1038/287447a0

Stockklausner, C., J. Ludwig, J.P. Ruppersberg, and N. Klöcker. 2001. A sequence motif responsible for ER export and surface expression of Kir2.0 inward rectifier K(+) channels. *FEBS Lett.* 493:129–133. https://doi.org/10.1016/S0014-5793(01)02286-4

Sutkowski, E.M., and W.A. Catterall. 1990. Beta 1 subunits of sodium channels. Studies with subunit-specific antibodies. *J. Biol. Chem.* 265: 12393–12399.

Terhag, J., N.A. Cavara, and M. Hollmann. 2010. Cave Canalem: how endogenous ion channels may interfere with heterologous expression in Xenopus oocytes. *Methods.* 51:66–74. https://doi.org/10.1016/j.ymeth.2010.01.034

Ukomadu, C., J. Zhou, F.J. Sigworth, and W.S. Agnew. 1992. muI Na+ channels expressed transiently in human embryonic kidney cells: biochemical and biophysical properties. *Neuron.* 8:663–676. https://doi.org/10.1016/0896-6273(92)90088-U

Ullrich, S., R. Gueta, and G. Nagel. 2013. Degradation of channelopsin-2 in the absence of retinal and degradation resistance in certain mutants. *Biol. Chem.* 394:271–280. https://doi.org/10.1515/hsz-2012-0256

Volkov, O., K. Kovalev, V. Polovinkin, V. Borshchevskiy, C. Bamann, R. Astashkin, E. Marin, A. Popov, T. Balandin, D. Willbold, et al. 2017. Structural insights into ion conduction by channelrhodopsin 2. *Science.* 358:eaan8862. https://doi.org/10.1126/science.aan8862

Wallner, M., L. Weigl, P. Meera, and I. Lotan. 1993. Modulation of the skeletal muscle sodium channel alpha-subunit by the beta 1-subunit. *FEBS Lett.* 336:535–539. https://doi.org/10.1016/0014-5793(93)80871-Q

Walzik, S., A. Schroeter, K. Benndorf, and T. Zimmer. 2011. Alternative splicing of the cardiac sodium channel creates multiple variants of mutant T1620K channels. *PLoS One.* 6:e19188. https://doi.org/10.1371/journal.pone.0019188

Weber, W.M. 1999. Endogenous ion channels in oocytes of xenopus laevis: recent developments. *J. Membr. Biol.* 170:1–12. https://doi.org/10.1007/s002329900532

Webster, G., and C.I. Berul. 2013. An update on channelopathies: from mechanisms to management. *Circulation.* 127:126–140. https://doi.org/10.1161/CIRCULATIONAHA.111.060343

West, J.W., T. Scheuer, L. Maechler, and W.A. Catterall. 1992. Efficient expression of rat brain type IIA Na+ channel alpha subunits in a somatic cell line. *Neuron.* 8:59–70. https://doi.org/10.1016/0896-6273(92)90108-P

Zimmer, T., and K. Benndorf. 2002. The human heart and rat brain IIA Na+ channels interact with different molecular regions of the beta1 subunit. *J. Gen. Physiol.* 120:887–895. https://doi.org/10.1085/jgp.20028703

Zimmer, T., and K. Benndorf. 2007. The intracellular domain of the beta 2 subunit modulates the gating of cardiac Na v 1.5 channels. *Biophys. J.* 92:3885–3892. https://doi.org/10.1529/biophysj.106.098889

Zimmer, T., and R. Surber. 2008. SCN5A channelopathies--an update on mutations and mechanisms. *Prog. Biophys. Mol. Biol.* 98:120–136. https://doi.org/10.1016/j.pbiomolbio.2008.10.005
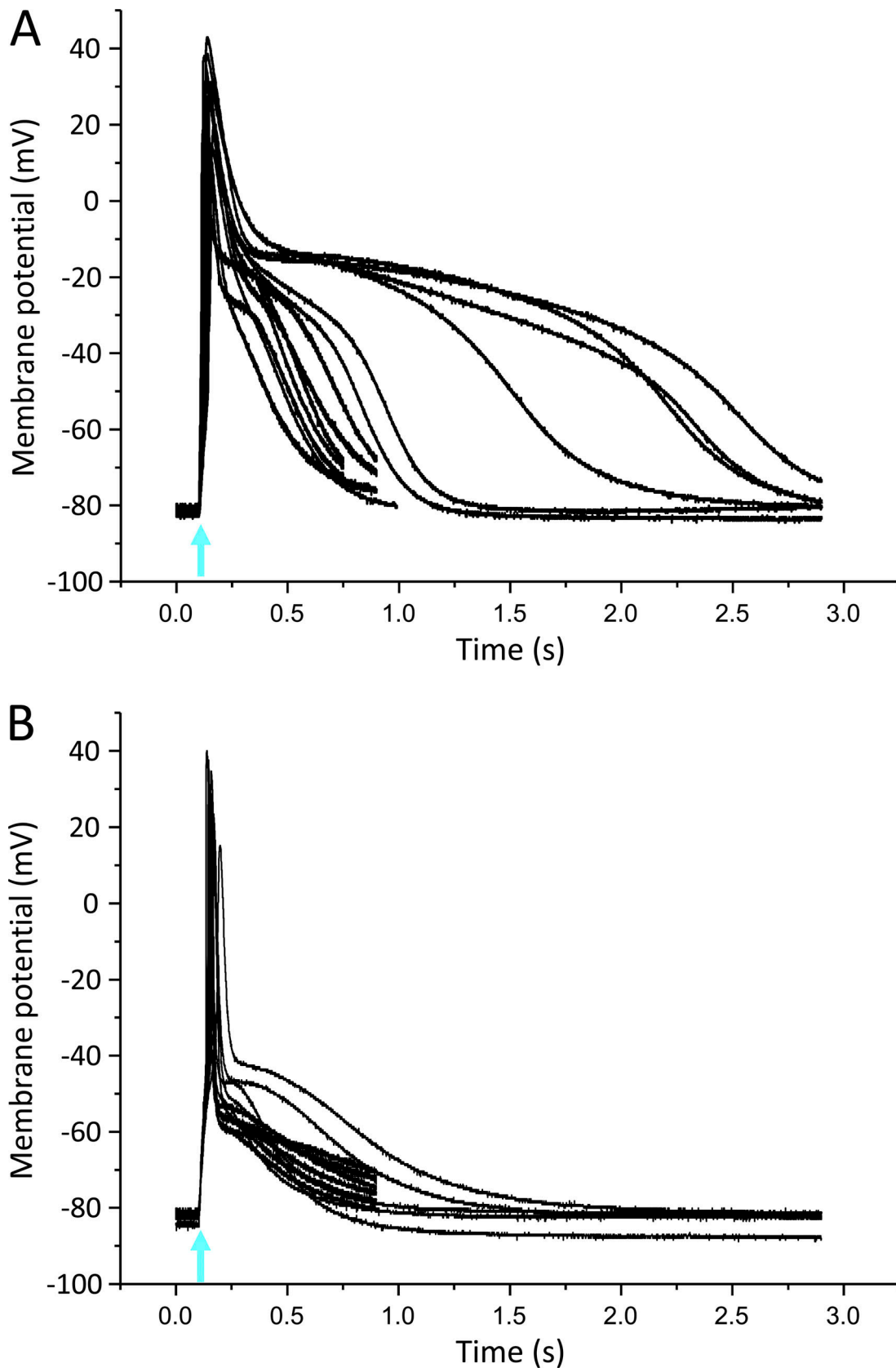
Supplemental material

Figure S1. **Light-induced APs in *Xenopus* oocytes using the skeletal muscle Na⁺ channel subtype Na$_v$1.4. (A)** Thirteen superimposed current-clamp recordings in oocytes expressing Na$_v$1.4 and β1-ChR2. **(B)** Eleven superimposed current-clamp recordings in oocytes expressing Na$_v$1.4, β1-ChR2, and K$_v$2.1. Coexpression of the voltage-gated K⁺ channel led to AP shortening and a less pronounced variability in AP duration and shape. For detailed statistics, see Table S1. The blue-light flash is indicated by an arrow.
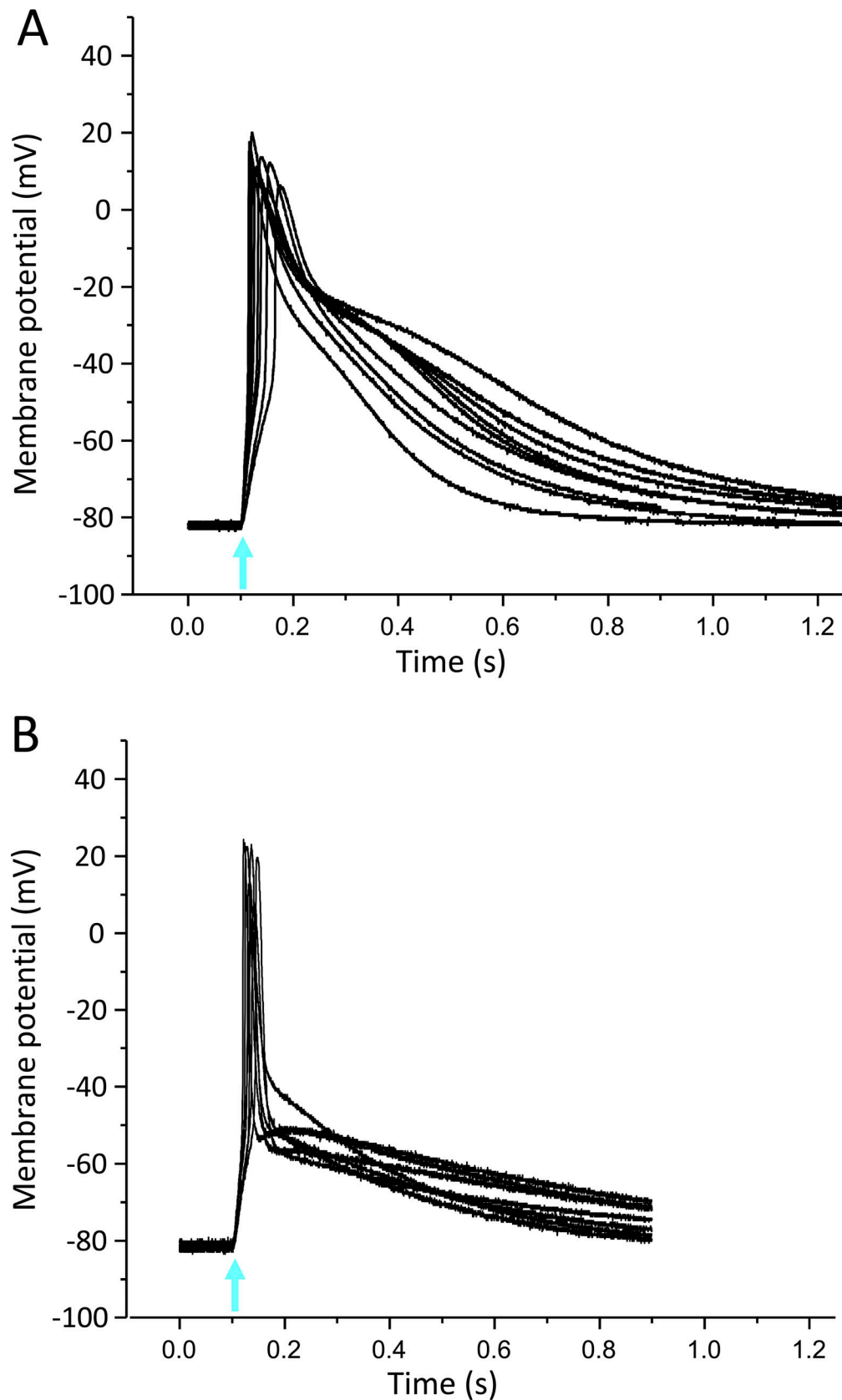
Figure S2. **Light-induced APs in *Xenopus* oocytes using the cardiac Na⁺ channel Na$_v$1.5. (A)** Nine superimposed current-clamp recordings in oocytes expressing Na$_v$1.5 and β1-ChR2. **(B)** Seven superimposed current-clamp recordings in oocytes expressing Na$_v$1.5, β1-ChR2, and K$_v$2.1. Similarly, as observed for Na$_v$1.4–injected oocytes, coexpression of K$_v$2.1 led to a pronounced AP shortening. For detailed statistics, see Table S2. The blue-light flash is indicated by an arrow.

Table S1 is provided online as a separate Word file and shows statistics on AP parameters for oocytes expressing either $Na_v1.4/\beta1$-ChR2 or $Na_v1.4/ \beta1$-ChR2/$K_v2.1$ channels. Table S2 is also provided online and shows statistics on AP parameters for oocytes expressing either $Na_v1.5/ \beta1$-ChR2 or $Na_v1.5/\beta1$-ChR2/$K_v2.1$ channels.